Neuronal Excitability

Recurring Cholinergic Inputs Induce Local Hippocampal Plasticity through Feedforward Disinhibition

Inês Guerreiro,[1] Zhenglin Gu,[2] Jerrel L. Yakel,[2] and Boris S. Gutkin[1,3]

[1]Group for Neural Theory, LNC2 INSERM U960, Département d'études cognitives, Ecole Normale Superieure, PSL Université Paris, 75005 Paris, France, [2]Neurobiology Laboratory, National Institute of Environmental Health Sciences, National Institutes of Health, Department of Health and Human Services, Research Triangle Park, North Carolina 27709, and [3]Center for Cognition and Decision Making, Institute for Cognitive Neuroscience, National Research University Higher School of Economics, Moscow 101000, Russia

Abstract

The CA1 pyramidal neurons are embedded in an intricate local circuitry that contains a variety of interneurons. The roles these interneurons play in the regulation of the excitatory synaptic plasticity remains largely understudied. Recent experiments showed that recurring cholinergic activation of $\alpha 7$ nACh receptors expressed in oriens-lacunosum-moleculare (OLM$\alpha 2$) interneurons can directly induce LTP in Schaffer collateral (SC)–CA1 synapses. Here, we pair *in vitro* studies with biophysically based modeling to uncover the underlying mechanisms. According to our model, $\alpha 7$ nAChR activation increases OLM GABAergic activity. This results in the inhibition of the fast-spiking interneurons that provide feedforward inhibition onto CA1 pyramidal neurons. This disinhibition, paired with tightly timed SC stimulation, can induce potentiation at the excitatory synapses of CA1 pyramidal neurons. Our work details the role of cholinergic modulation in disinhibition-induced hippocampal plasticity. It relates the timing of cholinergic pairing found experimentally in previous studies with the timing between disinhibition and hippocampal stimulation necessary to induce potentiation and suggests the dynamics of the involved interneurons plays a crucial role in determining this timing.

Key words: hippocampus; synaptic plasticity; disinhibition; Schaffer Collateral; nicotinic receptors; GABA neurons

Significance Statement

We use a combination of experiments and mechanistic modeling to uncover the key role for cholinergic neuromodulation of feedforward disinhibitory circuits in regulating hippocampal plasticity. We found that cholinergic activation of $\alpha 7$ nAChR expressed in oriens-lacunosum-moleculare interneurons, when tightly paired with stimulation of the Schaffer collaterals, can cancel feedforward inhibition onto CA1 pyramidal cells, enabling the potentiation of the SC–CA1 synapse. Our work details how cholinergic action on GABAergic interneurons can tightly regulate the excitability and plasticity of the hippocampal network, unraveling the intricate interplay of the hierarchal inhibitory circuitry and cholinergic neuromodulation as a mechanism for hippocampal plasticity.

Introduction

The hippocampal networks are characterized by a variety of locally connected GABAergic interneurons exerting robust control on network excitability. Previous work has detailed the importance of inhibitory inputs in modulating local hippocampal synaptic plasticity (Wigström and

Gustafsson, 1985; Meredith et al., 2003; Chevalerye and Piskorowski, 2014; Saudargienė and Graham, 2015). Furthermore, several experimental studies show that disinhibition facilitates the induction of long-term potentiation (LTP) at excitatory synapses (Ormond and Woodin, 2009; Yang et al., 2016). However, how the disinhibition controlling hippocampal excitatory synapses is modulated (e.g., by neuromodulators) is not clearly understood, and the precise circuitry and its dynamics underlying this type of plasticity remains an open question.

GABAergic interneurons receive significant cholinergic innervation from the medial septum. They are endowed with various subtypes of nicotinic ACh receptors (nAChRs) that regulate excitability, plasticity, and cognitive functions (Pitler and Alger, 1992; Behrends and Ten Bruggencate, 1993; Hasselmo et al., 1995; Alkondon et al., 1997; Patil et al., 1998; McQuiston and Madison, 1999; Patil and Hasselmo, 1999; Levin, 2002; Hasselmo, 2006; Parikh et al., 2007; Bell et al., 2011, 2015; Griguoli and Cherubini, 2012; Yakel, 2012; Desikan et al., 2018; Nicholson and Kullmann, 2021). Moreover, alterations of cholinergic action on hippocampal GABAergic interneurons have been implicated in cognitive dysfunction in Alzheimer's disease (AD; Schmid, et al., 2016). These studies, among others, furnish clear evidence that cholinergic inputs exert a powerful role in regulating hippocampal activity. Still, because of the abundance of cholinergic receptors (both muscarinic and nicotinic) and the complexity of the networks in which they are embedded, it is difficult to access the exact mechanisms through which cholinergic action on the hippocampus modulates its microcircuits.

Previous studies showed that activation of $\alpha7$ nACh receptors expressed in oriens-lacunosum-moleculare (OLM$\alpha2$) interneurons increases Schaffer collateral (SC)–CA1 transmission and suggest that this happens through disinhibition by reducing the activity of stratum radiatum (s.r.) interneurons that in turn provide feedforward inhibition onto pyramidal (PYR) neurons (Leão et al., 2012). Consistent with these studies, Gu et al. (2020) found that repeated coactivation of $\alpha7$ nAChR on OLM$\alpha2$ interneurons and a local SC pathway increased CA1 EPSCs and reduced IPSCs. However, the mechanisms through which the activation of the OLM$\alpha2$ interneurons regulates the activity of inhibitory interneurons targeting the CA1 pyramidal cell, and how this facilitates the increase of SC-evoked EPSPs of the CA1 pyramidal cells remain elusive.

In the CA1 region, $\alpha7$ nAChR can be found on both presynaptic and postsynaptic sites of GABAergic synapses (Fabian-Fine, 2001). For this reason, the outcome of $\alpha7$ nAChR activation and how it modulates OLM$\alpha2$ interneuron activity is difficult to address. Activation of postsynaptic $\alpha7$ nAChRs could increase the spiking frequency of OLM$\alpha2$ interneurons, although, to our knowledge, OLM$\alpha2$ spiking by nAChRs has not been clearly characterized, while presynaptic $\alpha7$ nAChRs regulate the release of neurotransmitter by activating calcium-dependent pathways that lead to the fusion of neurotransmitter vesicles with the membrane of the neuron (Desikan et al., 2018).

In this work, we use a minimal biophysical circuit model, driven quantitatively by *in vitro* data, to show how modulation of OLM cells (O-cells) influences the activity of fast-spiking interneurons whose GABAergic inputs are colocalized with the SC glutamatergic synapses onto a CA1 pyramidal cell dendrite, and how this promotes the induction of plasticity at the SC–CA1 synapse. We seek to determine how cholinergic activation of the OLM cells through presynaptic $\alpha7$ nAChRs can downregulate the GABAergic signaling onto the pyramidal cells, and how recurrent decreased inhibitory inputs can indirectly enhance the plasticity of the excitatory SC–CA1 synapse. We thus constructed a minimal circuit consisting of a single compartment spiking model of an OLM interneuron (O-cell) with $\alpha7$ nAChRs, a fast-spiking interneuron (I-cell) with AMPA and GABA$_A$ receptors, and a pyramidal cell dendritic compartment (E$_D$) with AMPA, NMDA, and GABA$_A$ receptors. They are connected as schematically shown in Figure 1.

Overwhelming evidence suggests that most types of LTP involve calcium influx through NMDARs and subsequent changes in the properties of postsynaptic AMPA receptors (AMPARs), namely changes in their number and phosphorylation state (Collingridge et al., 1983; Barria et al., 1997; Lüscher and Malenka, 2012). To reflect these mechanisms, we use the calcium-based synaptic plasticity model (proposed by Shouval et al., 2002) to model synaptic plasticity of the SC–CA1 excitatory synapse.

In this study, we use a combination of experiments with computational modeling to put together a coherent picture of the multiple mechanisms through which concurrent disinhibition directly induces local SC–CA1 plasticity. More specifically, we show how repeated concurrent disinhibition induces LTP by mediating AMPAR trafficking. Our modeling results also put together all the pieces of the puzzle to lay out how nAChR cholinergic action on OLM interneurons, working through calcium-dependent regulation of GABA neurotransmission, can downregulate the GABAergic signaling onto CA1 pyramidal cells and induce potentiation of the SC–CA1 synapse.

Materials and Methods

Animals and materials

All procedures related to the use of mice followed protocols approved by the Institutional Animal Care and Use Committees of the NIEHS. ChAT-cre mice [B6;129S6-
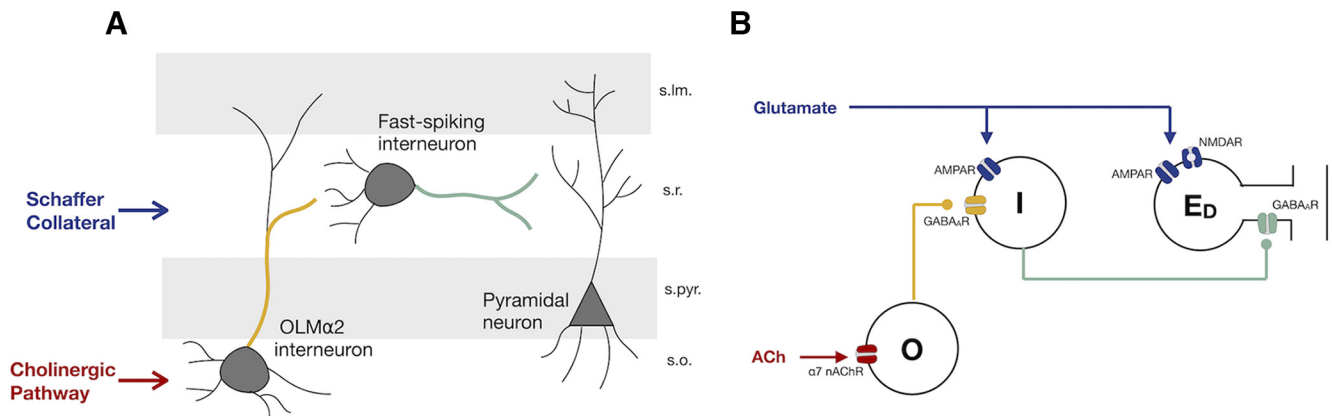
Figure 1. Disynaptic disinhibition circuit for nAChR-modulated long-term plasticity in the CA1. ***A***, Simplified wiring diagram of an interneuron network that mediates feedforward inhibition in the CA1 region of the hippocampus. Activation of the SC pathway leads to the activation of CA1 pyramidal cell dendrites and s.r. interneurons, which provide feedforward inhibition onto the pyramidal cell. Cholinergic activation of OLMα2 interneurons in s.o. leads to the inhibition of the s.r. interneurons, counteracting SC feedforward inhibition (Leão et al., 2012). ***B***, Minimal network to investigate plasticity induced by the pairing of cholinergic and SC activation. Glutamate activates postsynaptic AMPARs and NMDARs at the pyramidal cell E_D and postsynaptic AMPARs at I-cells, which in turn provide feedforward inhibition onto E_D by activating postsynaptic GABA$_A$Rs. Cholinergic inputs act on presynaptic α7 nAChRs of O-cells, which results in GABA release of the O-cells that it is going to bind to postsynaptic GABA$_A$Rs of the I-cell.

Chattm2(cre)Lowl/J], Sst-cre mice [Ssttm2.1(cre)Zjh], and floxed α7 nAChR knock-out mice [B6(Cg)-Chrna7tm1.1Ehs/YakelJ] were originally purchased from The Jackson Laboratory and then bred at the National Institute of Environmental Health Sciences (NIEHS). OLMα2-cre mice [Tg(Chrna2cre)OE29Gsat/Mmucd] were originally obtained from Mutant Mouse Resource and Research Centers and then bred at NIEHS. Mice (of either sex) were used for slice culture from day 6 to 8.

Culture media were from Sigma-Aldrich and Thermo Fisher Scientific. Adeno-associated virus (AAV) serotype 9 helper plasmid was obtained from James Wilson (University of Pennsylvania, Philadelphia, PA). The AAV vector containing floxed ChR2 (catalog #20297, Addgene) and floxed enhanced NpHR (eNpHR; catalog #26966, Addgene) were obtained from Karl Deisseroth (Stanford University, Palo Alto, CA; Gradinaru et al., 2010; Witten et al., 2010). AAV viruses were packaged with serotype 9 helper at the Viral Vector Core facility at the NIEHS.

Brain slice culture and AAV infection

To study the effects of cholinergic coactivation on the plasticity of SC–CA1 synapses (Fig. 2C,E), coronal septal slices (350 μm) from ChAT-cre mice and horizontal hippocampal slices from floxed α7 nAChR mice or OLMα2-cre/floxed α7 nAChR mice (350 μm) were cut with a vibratome (model VT1000S, Leica). Medial septal tissue containing cholinergic neurons was then dissected out and placed next to the hippocampus on a six-well polyester Transwell insert (Corning) and cultured there for ~2 weeks before being used for experiments, similar to those previously described (Gu and Yakel, 2017). AAVs containing a double-floxed ChR2 construct (5 nl) were microinjected to the septal tissue with a microinjector (Drummond Scientific) on the second day of culture. To study the effects of disinhibition on the plasticity of SC–CA1 synapses (see Fig.

4C), horizontal hippocampal slices from Sst-cre mice were cultured and AAVs containing double-floxed eNpHR construct were microinjected to the hippocampus the next day.

Whole-cell patch-clamp recordings

SC–CA1 EPSCs were recorded from hippocampal CA1 pyramidal neurons under whole-cell patch clamp, similar to recordings described in the studies by Gu and Yakel (2011, 2017). Briefly, 2–3 weeks after culturing, the slices were removed from transwell inserts and put into a submerged chamber, continuously perfused with 95% O$_2$/5% CO$_2$ balanced ACSF (in mM: 122 NaCl, 2.5 KCl, 2 MgCl$_2$, 2 CaCl$_2$, 1.2 NaH$_2$PO$_4$, 25 NaHCO$_3$, and 25 glucose) at room temperature. EPSCs were recorded at -60 mV under voltage clamp through a glass pipette filled with an internal solution (in mM: 130 potassium gluconate, 2 MgCl$_2$, 3 MgATP, 0.3 Na$_2$GTP, 10 KCl, 10 HEPES, and 1 EGTA) at pH ~7.2–7.3 and osmolarity of ~280–290 mOsm. Whole-cell patch-clamp recordings were performed with a Multiclamp 700B amplifier (Molecular Devices). Data were digitized with an analog-to-digital signal converter (Digidata 1550) and collected with Clampex. The amplitudes of EPSCs were analyzed with Clampfit, and graphs were drawn with Excel. The amplitudes were normalized to the mean of the 10 min baseline recording before cholinergic pairing or disinhibition pairing. Values were presented as the mean $\pm$ SEM.

EPSCs were evoked every 60 s by stimulating the SC pathway with an electrode placed in the stratum radiatum through a stimulator (model S88X, Grass). The stimulation intensity was 1–10 μA for 0.1 ms. To study the effects of cholinergic coactivation on SC–CA1 synaptic plasticity (Fig. 2C,E), cholinergic terminals in the hippocampus were optogenetically activated (10 pulses at 10 Hz, 1 s before SC stimulation) through ChR2 that was selectively
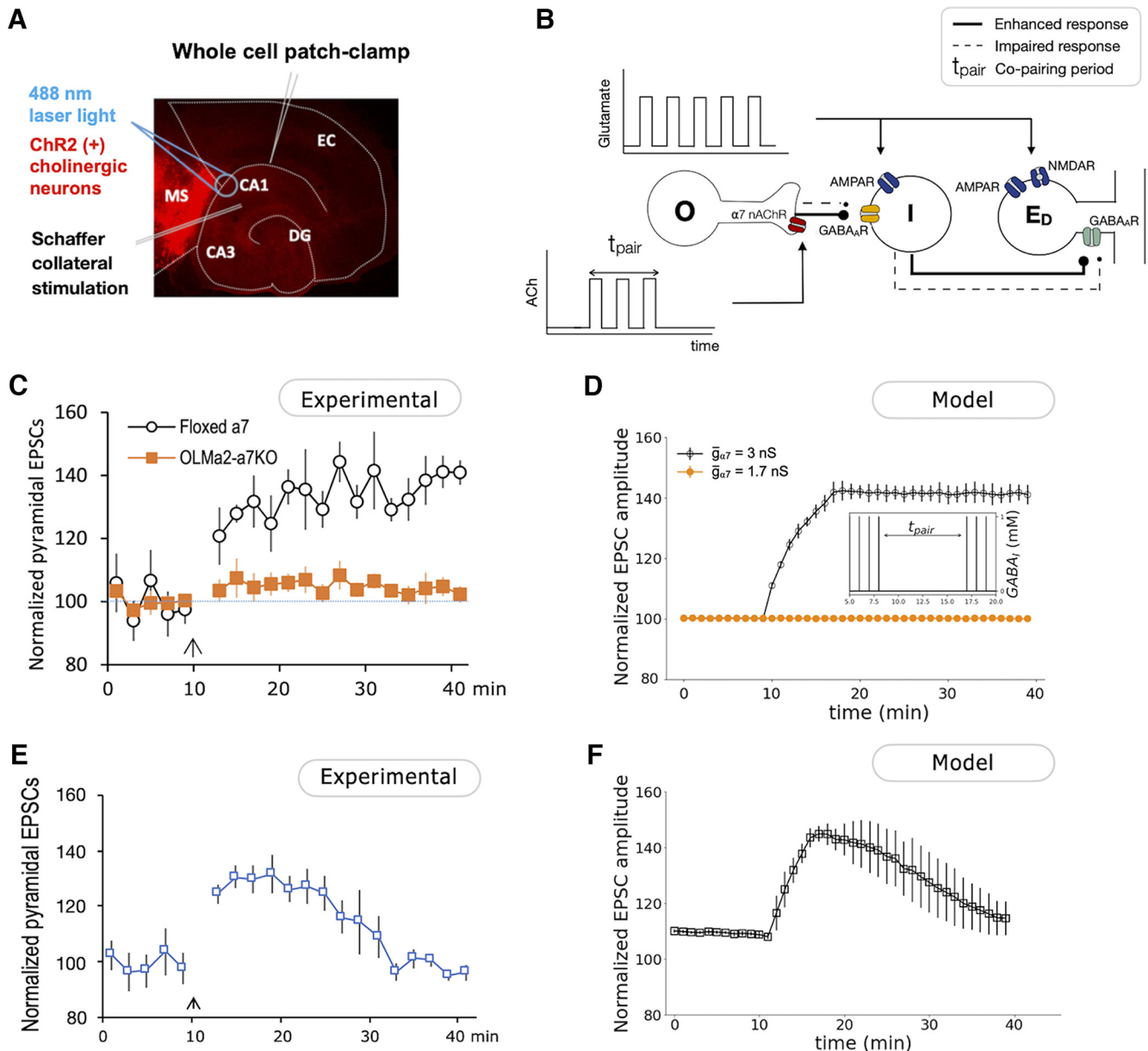
Figure 2. Cholinergic activation of OLM interneurons potentiates SC-evoked EPSCs. ***A***, Scheme of *in vitro* induction of cholinergic pairing-induced hippocampal synaptic plasticity. EPSCs were recorded from CA1 pyramidal neurons. Cholinergic neurons were activated via channelrhodopsin-2 that was specifically expressed in ChAT-positive neurons. The SC pathway was activated by a stimulating electrode. Adapted from the study by Gu et al. (2017). ***B***, Scheme of the minimal network used to study the role of cholinergic inputs in the potentiation of SC-evoked EPSCs. Glutamatergic inputs activate the pyramidal cell E_D and the fast-spiking I-cell that projects to it. Square pulses of ACh activate the O-cell during the copairing period. The neural response of O-cell, I-cell, and E_D when the system receives one pulse of glutamate paired or not with ACh is shown in Extended Data Figure 2-1. The release of GABA from the O-cells is calculated using the simplified model described by Equation 16. The Extended Data Figure 2-2 shows that the simplified neurotransmitter release model results in a similar synaptic activation function as the detailed model described in the study by Destexhe et al. (1998). Different ACh synaptic profiles are explored in Extended Data Figure 2-3. ***C***, Normalized SC-evoked EPSC responses from CA1 pyramidal neurons showing that the enhancement of EPSCs was impaired in hippocampal slices from mice with selective $\alpha 7$ nAChR knockout in OLM$\alpha 2$ interneurons. Adapted from the study by Gu et al. (2020). ***D***, Numerical simulation of normalized EPSC amplitude when glutamatergic inputs acting on the I-cell and E_D are paired with cholinergic inputs acting on the O-cell (from $t = 10$ min to $t = 18$ min). The EPSCs are calculated as the sum of postsynaptic AMPA and NMDA currents, I_{AMPA} and I_{NMDA}, resulting from 10 simulations with white noise on the E_D membrane potential. Noisy membrane potentials of the O-cells and I-cells that induce spontaneous spiking are considered in Extended Data Figure 2-4. Normalization of the results was calculated according with the expression (100 + (EPSC – EPSCmin) · (150–100))/(EPSCmax – EPSCmin). Inset, Concentration of GABA released from fast-spiking interneurons (I), calculated according to Equation 15 (see Materials and Methods). ***E***, Normalized SC-evoked EPSC responses from CA1 pyramidal neurons showing that enhancement of EPSCs during a copairing period of 5 min. ***F***, Numerical simulation of normalized EPSC amplitude when glutamatergic inputs acting on the I-cell and E_D are paired with cholinergic inputs acting on the O-cell (from $t = 10$ min to $t = 15$ min).

expressed in ChAT-cre-positive (cholinergic) neurons. ChR2 was activated with 488 nM laser light (5 mW, 20 ms) through a 40× objective over CA1 stratum oriens (s.o.) near the septum with an spinning disk confocal microscope (Andor Technology). To examine the effects of disinhibition on SC–CA1 synaptic plasticity (see Fig. 4C), somatostatin (Sst)-positive neurons were inhibited optogenetically through eNpHR which was activated through a 40× objective over CA1 stratum oriens with 530 nM laser light (20 mW) for 1 s flanking SC stimulation.

The amplitudes of EPSCs were analyzed with Clampfit, and graphs were drawn with Excel. The amplitudes were normalized to the mean of the 5 min baseline recording before cholinergic pairing or disinhibition pairing. Values were presented as the mean ± SEM EPSC amplitudes at 5 and 30 min after pairing were compared with the amplitude at 5 min before pairing. The effect at 5 min after pairing was considered to be a short-term effect, and the effect at 30 min after pairing was considered to be a long-term effect. Recordings were performed in five slices from three individual mice in each group. Statistical significance was tested by Student's t test. The sample size was estimated by Student's t test with an expected effect of 40% change, an expected SD of 15%, and an 80% confidence interval width.

Model

The minimal network used in this study consists of an O-cell, a fast-spiking I-cell, and a pyramidal cell. All the cells in the network are modeled as point neurons. Since we are interested in the local changes at the SC–CA1 synapse, the pyramidal cell is represented by a dendritic compartment (E_D). The cells of the network are connected through feedforward connections. Although recurrent connections from the CA1 pyramidal cell and the fast-spiking interneurons may exist, adding this connection did not change our results. Adding connections between the CA1 pyramidal cell and the OLM interneuron also did not significantly alter our results. Therefore, we did not include synapses between the CA1 pyramidal and the OLM cells in our model. Our modeling choice is further supported by experimental studies showing that the IPSC elicited by an OLM interneuron has a small amplitude at the soma of CA1 pyramidal cells since these synapses are on the distal parts of the dendritic tree (Maccaferri, et al., 2000), and that an action potential in CA1 pyramidal cells is insufficient to make the OLM cell membrane potential (V_m) cross the action potential threshold (Ali et al., 1998; Müller and Remy, 2014). Although repeated firing of CA1 pyramidal cells with theta frequency can facilitate excitatory inputs onto OLM, a theta activation protocol of the CA1 cell is beyond the scope of this article.

Neuron dynamics models

The O-cells and I-cells are modeled following the Hodgkin–Huxley formalism [Hodgkin and Huxley, 1952; transient (I_{Na}), delayed rectifier potassium (I_K), and leak (I_{leak})], with synaptic currents (I_{syn}). Its V_m is described as follows:

$$C_m \frac{dV_m}{dt} = -I_{leak} - I_K - I_{Na} - I_{syn}, \tag{1}$$

where C_m is the membrane capacitance. The I_{leak}, I_K, and I_{Na} currents are given by:

$$I_{leak} = g_{leak}(V_m - E_{leak}), \tag{2}$$

$$I_K = \bar{g}_K n^4 (V_m - E_K), \tag{3}$$

$$I_{Na} = \bar{g}_{Na} m^3 h (V_m - E_{Na}), \tag{4}$$

where $\bar{g}_i$ and E_i are, respectively, the maximal conductance and reversal potential of channel i (i = leak, K, Na), and m, h, and n are gating variables that obey the following differential equation:

$$\frac{dx}{dt} = \alpha_x(1-x) - \beta_x x, \tag{5}$$

where α_x and β_x are voltage-dependent rate constants.

Following Rotstein et al. (2005), we included an applied current (I_{app}) = −260 pA, a persistent Na current (I_p), and a hyperpolarization-activated inward current (I_h; with a slow and fast component) on the O-cells, as follows:

$$I_p = \bar{g}_p p (V_m - E_{Na}), \tag{6}$$

$$I_h = \bar{g}_h (0.65 h^f + 0.35 h^s)(V_m - E_h). \tag{7}$$

While the gate variable p obeys Equation 5, h^f and h^s are described by the following equation:

$$\frac{dx}{dt} = \frac{x_\infty(V_m) - x}{\tau_x(V_m)}, \tag{8}$$

where x_∞ is the voltage-dependent steady state and τ_x is the time constant. Definitions for the α_x, β_x, x_∞, and τ_x for each of the dynamic variables are as follows.

For the O-cells:

$$\alpha_n = \frac{-0.01(V_m + 27)}{\exp\left(-0.1(V_m + 27)\right) - 1},$$

$$\beta_n = 0.125 \exp\left(-\frac{V_m + 37}{80}\right),$$

$$\alpha_m = \frac{-0.1(V_m + 23)}{\exp\left(-0.1(V_m + 23)\right) - 1},$$

$$\beta_m = 4 \exp\left(-\frac{V_m + 48}{18}\right),$$

$$\alpha_h = 0.07 \exp\left(-\frac{V_m + 37}{20}\right),$$

$$\beta_h = \frac{1}{\exp(-0.1(V_m + 7) + 1)},$$

$$\alpha_p = \frac{1}{0.15\left(1 + \exp\left(-\dfrac{V_m + 38}{6.5}\right)\right)},$$

$$\beta_p = \frac{\exp\left(-\dfrac{V_m + 38}{6.5}\right)}{0.15\left(1 + \exp\left(-\dfrac{V_m + 38}{6.5}\right)\right)},$$

$$h_\infty^f = \frac{1}{1 + \exp\left(\dfrac{V_m + 79.2}{9.78}\right)},$$

$$\tau_h^f = \frac{0.51}{\exp\left(\dfrac{V_m - 1.7}{10}\right) + \exp\left(-\dfrac{V_m + 340}{52}\right)} + 1,$$

$$h_\infty^s = \frac{1}{\left[1 + \exp\left(\dfrac{V_m + 2.83}{15.9}\right)\right]^{58}},$$

$$\tau_h^s = \frac{5.6}{\exp\left(\dfrac{V_m - 1.7}{14}\right) + \exp\left(-\dfrac{V_m + 260}{43}\right)} + 1.$$

For the I-cells:

$$\alpha_n = \frac{0.032(V_m + 52)}{1 - \exp\left(-\dfrac{V_m + 52}{5}\right)},$$

$$\beta_n = 0.5\exp\left(-\dfrac{V_m + 57}{40}\right),$$

$$\alpha_m = \frac{0.32(V_m + 54)}{1 - \exp\left(-\dfrac{V_m + 54}{4}\right)},$$

$$\beta_m = \frac{0.28(V_m + 27)}{\exp\left(\dfrac{V_m + 27}{5}\right) - 1},$$

$$\alpha_h = 0.128\exp\left(-\dfrac{V_m + 50}{18}\right),$$

$$\beta_h = \frac{4}{1 + \exp\left(-\dfrac{V_m + 27}{5}\right)}.$$

The parameter values used in the simulations are the ones presented in Table 1.

Since we are interested in studying local synaptic changes of the SC–CA1 synapse, we use the following equation to describe the activity of the pyramidal cell dendritic compartment:

Table 1: Parameters of pyramidal cell, OLM interneuron, and fast-spiking interneuron dynamics

Parameter	Value
O-cells	
C_m	100 pF
g_{leak}	50 nS
E_{leak}	−70 mV
$\bar{g}_K$	1100 nS
E_K	−90 mV
$\bar{g}_{Na}$	5200 nS
E_{Na}	55 mV
$\bar{g}_p$	50 nS
$\bar{g}_h$	145 nS
E_h	−20 mV
I-cells	
C_m	100 pF
g_{leak}	10 nS
E_{leak}	−67 mV
$\bar{g}_K$	8000 nS
E_K	−100 mV
$\bar{g}_{Na}$	10,000 nS
E_{Na}	50 mV
E_D	
C_m	100 pF
g_{leak}	1 nS
E_{leak}	−68 mV

All the parameter values and expressions here described were taken from the study by Rotstein et al. (2005), considering a surface area of 1×10^{-4} cm^2, except for the reversal potential of the leakage current of the OLM, which was set to have the resting potential of the OLM cells at −60 mV, as reported in the study by Leão et al. (2012).

$$C\frac{dV_{ED}}{dt} = -I_{leak} - I_{syn}. \tag{9}$$

The parameters C, g_{leak}, and E_{leak} were set to 100 pF, 1 nS, and −68 mV, respectively.

For the simulations presented in Figure 2D, noise was added to the dendritic compartment E_D to allow direct comparison with the experimental results portrait in Figure 2C. In addition to E_D, white noise was added to the O-cells and I-cells to study plasticity induction when these cells show spontaneous spiking (Extended Data Figs. 2-1, 2-2, 2-3, 3-1, 3-2, 4-1). Since we used the Euler method to solve the differential equations describing V_O, V_I, and V_{ED}, $(V_x[i + 1] = V_x[i] + dt\frac{dV_x}{dt})$ noise was incorporated by adding a stochastic term $\sqrt{dt}\zeta$ $(V_x[i + 1] = V_x[i] + dt\frac{dV_x}{dt} + \sqrt{dt}\zeta)$, where ζ is a random Gaussian variable with mean $\mu = 0$ and SD σ(=1.1, 0.1, and 0.3 for the O-cells, I-cells, and E_D cells, respectively).

Synaptic models

The O-cell model includes a current mediated by $\alpha7$ nAChR channels, which in the real OLM neurons are presynaptic to the O-cell to I-cell synapse. The description of the current used is an adaptation of the model proposed in the study by Graupner et al. (2013), and it is given by the following equation:

$$I_{\alpha7} = \bar{g}_{\alpha7}r_{\alpha7}(V_m - E_{\alpha7}), \tag{10}$$

where $\bar{g}_{\alpha7}$ is the maximal conductance of the $\alpha7$ nAChR channel, and $E_{\alpha7}$ is the reversal potential. The opening

gate variable $r_{\alpha 7}$ is described by Equation 8, with $\tau_{r\alpha 7}$ (= 5 ms) constant and $r_{(\alpha 7)\infty}$ given by the following:

$$r_{(\alpha 7)\infty} = \frac{[ACh]^n}{EC_{50}^n + [ACh]^n}, \qquad (11)$$

where n is the Hill's coefficient of activation.

The I-cell has excitatory AMPA and inhibitory GABA$_A$ synaptic currents, described by the following set of equations:

$$I_{GABA_A} = \bar{g}_G r_G (V_m - E_G), \qquad (12)$$

$$I_{AMPA} = \bar{g}_{AMPA} r_A (V_m - E_A). \qquad (13)$$

The gating variable r_x is, as described in the study by Destexhe et al. (1998), given by the following:

$$\frac{dr_x}{dt} = \alpha_x [T](1 - r_x) - \beta_x r_x, \qquad (14)$$

where α_x and β_x are the opening and closing rates of the receptor channel, and [T] is the concentration of the neurotransmitter that is available for binding.

The GABA released by the I-cell is described by using the Destexhe et al. (1998) simplified neurotransmitter release model. The intervening reactions in the release process are considered to be fast: a presynaptic action potential elicits a rapid influx of calcium, leading to the activation of transmitter-containing vesicles and neurotransmitter release. A stationary relationship between presynaptic voltage and neurotransmitter release is deduced by fitting the model to experimental results. The following equation gives the neurotransmitter release as a function of the presynaptic voltage:

$$[GABA]_I = \frac{T_{max}}{1 + \exp\left(-\frac{V_m - V_p}{K_p}\right)}, \qquad (15)$$

where T_{max} = 1 mM is the maximal neurotransmitter concentration, K_p = 5 mV gives the steepness of the function, and V_p = 2 mV sets the value at which the function is half-activated. These parameters were directly taken from the study by Destexhe et al. (1998).

Spiking of the OLM cells directly because of the nAChR activation has not been clearly characterized. Experimentally measured nicotinic responses of OLM cells are small (Leão et al., 2012), and, although they may modulate the firing rate of the neuron, it is unlikely they are causing spiking on their own (Fig. 2D). For that reason, we consider that GABA release by the O-cell results from the activation of presynaptic $\alpha 7$ nAChR on O–I GABAergic synapses.

Experimental studies revealed that the activation of $\alpha 7$ nAChRs trigger intracellular calcium rise and calcium-dependent signaling pathways—in particular calcium-induced calcium release (CICR) from intracellular stores—that enhance the release of neurotransmitter at presynaptic terminals (Tsuneki et al., 2000; Dajas-Bailador et al., 2002; Griguoli and Cherubini, 2012). To avoid the detailed computation of the mechanisms whereby calcium leads to exocytosis, we assume a sigmoid relationship between intracellular calcium and transmitter concentration given by the following:

$$[GABA]_O = \frac{T_{max}}{1 + \exp\left(-\frac{Ca_i - Ca_p}{K_{(Ca)p}}\right)}, \qquad (16)$$

where T_{max} = 1 mM is the maximal neurotransmitter concentration, $K_{(Ca)p} = 1 \times 10^{-6}$ mM gives the steepness of the function, and $Ca_p = 4 \times 10^{-5}$ mM sets the value at which the function is half-activated. These parameters were chosen so that a pulse of calcium elicits GABA release with approximately the same characteristics (amplitude and duration) as the detailed model of transmitter release in the study by Destexhe et al. (1998; Extended Data Fig. 2-2, compare detailed and simplified models of neurotransmitter release). Note that although Ca_p is below the calcium resting values typically observed, in our model the calcium concentration decays to zero, similar to that in the studies by Graupner and Brunel (2005, 2012), Higgins et al. (2014), and Shouval et al. (2002).

The passive dendritic compartment of the pyramidal cell E_D is modeled using synaptic GABA$_A$, AMPA, and NMDA currents. The GABA$_A$ and AMPA currents are given by Equations 12 and 13, respectively. The following equation describes the NMDA current:

$$I_{NMDA} = \bar{g}_N r_N B(V_m)(V_m - E_N), \qquad (17)$$

where r_N is the gating variable described by Equation 14. Because of the presence of an Mg^{2+} block, the NMDA channels have an additional voltage-dependent term, $B(V_m)$, defined as follows:

$$B(V_m) = \frac{1}{1 + \exp(-0.062 V_m)\frac{[Mg^{2+}]}{3.57}}. \qquad (18)$$

The parameters α_A, β_A, E_A, α_N, β_N, E_N, [Mg^{2+}], α_G, β_G, and E_G were estimated by Destexhe et al. (1998) by fitting the models of postsynaptic AMPA, NMDA and GABA$_A$ currents to experimental data. Regarding the synaptic currents of E_D, the maximal conductances of AMPA and NMDA receptors were chosen such that at $V = -70$ mV, a glutamate pulse of 1 mM and 10 ms duration evoked AMPA and NMDA currents with amplitudes of 240 and 40 pA, respectively (Andrásfalvy et al., 2003). The maximal conductance of GABA$_A$ receptors was chosen such that at $V = 0$ mV a pulse of GABA with 1 ms duration and a concentration of 1 mM evokes a current with an amplitude of 500 pA (Schulz et al., 2018). For the I-cell, the AMPA receptor maximal conductance value is such that one pulse of glutamate coming from the SC evokes a volley of action potentials. Concerning the $\alpha 7$ nAChR postsynaptic current, the parameters EC$_{50}$, $\tau_{r\alpha 7}$, and n were taken from the study by Graupner et al. (2013), where the kinetics of $\alpha 7$ nAChR is described. The parameter $E_{\alpha 7}$ was deduced from the study by Castro and Albuquerque (1995), and g$\alpha 7$ was chosen such that activation of the $\alpha 7$ nAChR by a pulse of ACh evokes a current of 35 pA (Leão et al., 2012). The values of the parameters can be found in Table 2.

Table 2: Parameter values of synaptic currents I_{AMPA}, I_{NMDA}, I_{GABAA}, and $I_{\alpha 7}$

Parameter	Value	Reference
α_A	$1.1\ \mathrm{ms^{-1}\ mM^{-1}}$	Destexhe et al. (1998)
β_A	$0.19\ \mathrm{ms^{-1}}$	Destexhe et al. (1998)
$\bar{g}_{AMPA}$	$7^*, 4^{\dagger}$ nS	Andrásfalvy et al. (2003)
E_A	0 mV	Destexhe et al. (1998)
$[Mg^{2+}]$	1 mM	Destexhe et al. (1998)
α_N	$0.072\ \mathrm{ms^{-1}\ mM^{-1}}$	Destexhe et al. (1998)
β_N	$6.6 \times 10^{-3}\ \mathrm{ms^{-1}}$	Destexhe et al. (1998)
$\bar{g}_N$	25 nS	Andrásfalvy et al. (2003)
E_N	0 mV	Destexhe et al. (1998)
α_G	$5\ \mathrm{ms^{-1}\ mM^{-1}}$	Destexhe et al. (1998)
β_G	$0.18\ \mathrm{ms^{-1}}$	Destexhe et al. (1998)
$\bar{g}_G$	$14^*, 7^{\dagger}$ nS	Schulz et al. (2018)
E_G	-80 mV	Destexhe et al. (1998)
$E_{\alpha 7}$	0 mV	Castro and Albuquerque (1995)
$\bar{g}_{\alpha 7}$	3 nS	Leão et al. (2012)
EC_{50}	80×10^{-3} mM	Graupner et al. (2013)
$\tau_{r\alpha 7}$	5 ms	Graupner et al. (2013)
n	1.73	Graupner et al. (2013)
T_{max}	1 mM	Destexhe et al. (1998)
K_p	5 mV	Destexhe et al. (1998)
V_p	2 mV	Destexhe et al. (1998)
$K_{(Ca)p}$	1×10^{-6} mM	Materials and Methods
Ca_p	4×10^{-5} mM	Materials and Methods

*Values refer to the conductance of postsynaptic channels on the fast-spiking interneurons.
†Values refer to the conductances of the dendritic compartment E_D.

CICR mechanism

Calcium entry through $\alpha 7$ nAChRs initiates calcium release from internal stores (Tsuneki et al., 2000; Dajas-Bailador et al., 2002; Griguoli and Cherubini, 2012). The calcium concentration in the cytosol of OLM cells (Ca_i) is described by the following equation:

$$\frac{dCa_i}{dt} = -\xi' \alpha' I_{\alpha 7} + w_{\infty}^3 (Ca_{IS} - Ca_i) - \frac{Ca}{\tau_{Ca}}, \quad (19)$$

where $\xi' = 2.1 \times 10^{-6}$ ^{mm}/(ms pA) is a parameter that converts current into concentration, $\alpha' = 0.05$ reflects the 5% calcium permeability of the $\alpha 7$ nAChRs (Vernino et al., 1994), and τ_{Ca} is the calcium decay constant. The parameter ξ' was chosen so that the intracellular calcium concentration is of the same order of magnitude as observed experimentally in the study by Sabatini et al. (2002; i.e., in the 0.1 μM range). The parameter τ_{Ca} was taken directly from the same study. Ca_{IS} represents the calcium concentration of the internal stores given by the following:

$$\frac{dCa_{IS}}{dt} = -w_{\infty}^3 (Ca_{IS} - Ca_i) - \frac{(Ca_{IS} - 0.44 \times 10^{-3})}{\tau}, \quad (20)$$

where τ (= 10 ms) is the calcium decay constant, and w_{∞} is the open probability of calcium-permeable channels on the internal store, given by the following:

$$w_{\infty} = \frac{Ca_i}{Ca_i + k_d}, \quad (21)$$

where k_d (= 2×10^{-4} ^{mm}) is the half-activation of the function. The model assumes three calcium binding sites

(Young and Keizer, 1992) and a calcium concentration at the internal stores of 0.44 μM at rest (this value can be different as long as it is bigger than the intracellular calcium concentration Ca_i). Please note that the CICR mechanism described is a simplification of the model proposed by Rinzel (1985), where we limit the model to account for the calcium activation sites of the calcium-permeable IP_3 receptors on the endoplasmic reticulum.

Model of synaptic plasticity

To study plasticity induction at the SC–E_D synapse, we use a calcium-based synaptic plasticity model based on the study by Shouval et al. (2002). We assume that changes in the AMPA receptor conductance reflect changes in the strength of the excitatory SC–CA1 synapse. Our synaptic plasticity model is formulated as follows:

$$\frac{d\bar{g}_{AMPA}}{dt} = \eta(Ca)\Big(\Omega(Ca) - \sigma(\bar{g}_{AMPA} - g_0)\Big), \quad (22)$$

where σ is a decay constant and g_0 (= 4 nS) is the value of the maximal conductance of the AMPAR at $t = 0$. The variable η is a calcium-dependent learning rate described by Equation 23, and Ω determines the sign magnitude of synaptic plasticity as a function of the intracellular Ca levels (Eq. 24).

$$\eta(Ca) = \left(\frac{P_1}{P_2 + Ca^{P_3}} + P_4\right)^{-1}, \quad (23)$$

$$\Omega(Ca) = \gamma_{\uparrow} \frac{\exp\big(900(Ca - \theta_{\uparrow})\big)}{1 + \exp\big(900(Ca - \theta_{\uparrow})\big)} - \gamma_{\downarrow} \frac{\exp\big(900(Ca - \theta_{\downarrow})\big)}{1 + \exp\big(900(Ca - \theta_{\downarrow})\big)}. \quad (24)$$

The parameters $\theta_{\uparrow}$ and $\theta_{\downarrow}$ define the potentiation and depression onset (i.e., the calcium levels that trigger the removal and insertion of AMPAR in the membrane, respectively), and $\gamma_{\uparrow}$ and $\gamma_{\downarrow}$ represent the maximal insertion and removal rate of the AMPARs from the membrane. Please note that on the original model, the parameters $\theta_{\uparrow}$ and $\theta_{\downarrow}$ are represented by θ_p and θ_d, and define the potentiation and depression threshold, respectively, but, as will be evident in the Results section, we find that this terminology can be misleading (i.e., we show that crossing these levels is necessary but not sufficient for potentiation).

We assume that the primary source of Ca^{2+} in E_D is the calcium flux entering the cell through the NMDA receptor channels. The intracellular Ca^{2+} concentration evolves according to the following equation:

$$\frac{dCa}{dt} = -\xi \alpha I_{NMDA} - \frac{Ca}{\tau_{Ca}}, \quad (25)$$

where ξ is a parameter that converts current into concentration, $\alpha = 0.1$ refers to the fact that only ~10% of the

NMDA current is composed of calcium ions (Burnashev et al., 1995), and τ_{Ca} (= 12 ms) refers to the calcium decay constant. The parameter ξ was chosen so that the intracellular calcium concentration is of the same order of magnitude as observed experimentally in the study by Sabatini et al. (2002). The parameter τ_{Ca} was taken directly from the same study. P_1, P_2, P_3, and P_4 were chosen to have a calcium-dependent learning rate that increases monotonically with calcium levels (Shouval et al., 2002). The parameters $\theta_\uparrow$ and $\theta_\downarrow$ were determined such that before the copairing period the calcium concentration does not cross either while crossing the potentiation onset $\theta_\uparrow$ when pairing starts (with $\theta_\uparrow > \theta_\downarrow$). The parameters σ, $\gamma_\uparrow$ and $\gamma_\downarrow$ were chosen to reproduce the experimental results concerning potentiation of CA1 PYR cell EPSC during coactivation of SC and disinhibition/cholinergic inputs (with $\gamma_\uparrow > \gamma_\downarrow$).

Stimulation protocol

ACh–SC pairing

We constructed a minimal feedforward circuit with an O-cell, a fast-spiking I-cell, and the pyramidal cell s.r. E_D connected, as schematically shown in Figure 2B, to examine mechanistically how pairing cholinergic activation of the O-cell with glutamatergic activation of the I-cell and E_D can potentiate the EPSCs of E_D. We look at how the EPSC of E_D, modeled as the sum of the postsynaptic AMPA current (I_{AMPA}) and NMDA current (I_{NMDA}), changes when the glutamatergic inputs acting on the I-cell and E_D are paired with the cholinergic inputs that act on the presynaptic $\alpha7$ nAChR of the O-cell during a copairing period of 5 and 8 min, identical to the experimental protocol. The I-cell and E_D receive one glutamate pulse per minute before, during, and after the copairing period. During the copairing period, the O-cell gets a pulse of ACh per minute, 100 ms before each glutamate pulse ($\Delta t = 100$ ms). Not much is known about the concentration profile of ACh *in vivo*, but it is believed that it can be cleared from the synaptic cleft within milliseconds. After testing different ACh profiles, we decided to model ACh as a square pulse with a duration of 5 ms and concentration of 1 mM, similar to glutamate, although similar results were obtained for a variety of profiles of ACh (Extended Data Fig. 2-3, for more details).

We explore the copairing temporal parameters that regulate plasticity by fixing the frequency of stimulations at 1 pulse/min while varying the copairing period t_{pair} (Figs. 2, 3A, results). We also study how the frequency of stimulation modulates synaptic plasticity by fixing t_{pair} at 4 min while changing the frequency of copaired stimulation (Fig. 3B). Finally, we consider different pairing times of ACh and glutamate (Δt; Fig. 3C,D).

Disinhibition–SC pairing

To study the disinhibitory mechanism of plasticity induction, we consider the dendritic compartment E_D subjected to glutamate and GABA pulses, as schematically shown in Figure 4B. Both GABA and glutamate are modeled as square pulses with a duration of 1 ms and 1 mm of amplitude (Extended Data Fig. 4-2A, different durations and amplitudes of glutamate and GABA reproduce the

same results), and a frequency of 1 pulse/min, with glutamate preceding GABA by 2 ms.

Parameters of the model

We used experimentally determined values or values from previous modeling studies for most of the parameters. Parameters that could not be set experimentally were determined by experimental constraints imposed on the model, namely, the maximal conductances $\bar{g}_x$, and the synaptic plasticity model parameters are indicated with a dash in Table 3.

All the parameter values are defined in Tables 1, 2, and 3. We strived to constrain the parameters to physiological values based on literature, those parameters that we could not directly constrain, were optimized to ranges that ensure that our simulations showed that the measurable variables used are within the physiological range.

We note that different sets of parameters can reproduce our results (Extended Data Fig. 4-2), and that they can be more finely tuned as more experimental data are collected and more constraints are imposed on the model. This also applies for the description of the neurotransmitters ACh, GABA, and glutamate. Despite not having access to data regarding their profile in the synaptic cleft during the experiments performed, we note that the profiles of different neurotransmitters can reproduce our results. In some cases, it may require that free parameters such as ξ and ξ', the parameters that convert currents into the calcium concentration, are readjusted to keep calcium within the electrophysiological range. In addition, for the particular case of the ACh dynamics, much higher concentrations than the ones considered here may require a more detailed description of the CICR mechanism by, for example, adding a calcium pump to the membrane of the internal stores and the OLM neuron to control the calcium flux into the intracellular medium.

We approximate the solutions of the differential equations with the Euler's method. We use a step size of 0.02 ms, which is the biggest value for which we have nonerratic solutions. To ensure the stability of our numerical method, we ran a number of pilot simulations with a smaller time step. We found that, for example, a timestep of 0.01 ms did not produce different results, while increasing considerably the time of computation.

Code accessibility

The code described in the article is freely available at https://github.com/inesCompleto/Hippocampal_Plasticity.

Data availability

The data that support the findings of this study (Gu et al., 2020) are available from the corresponding author on reasonable request.

Results

Coactivation of cholinergic and glutamatergic inputs modifies the SC-CA1 synaptic transmission

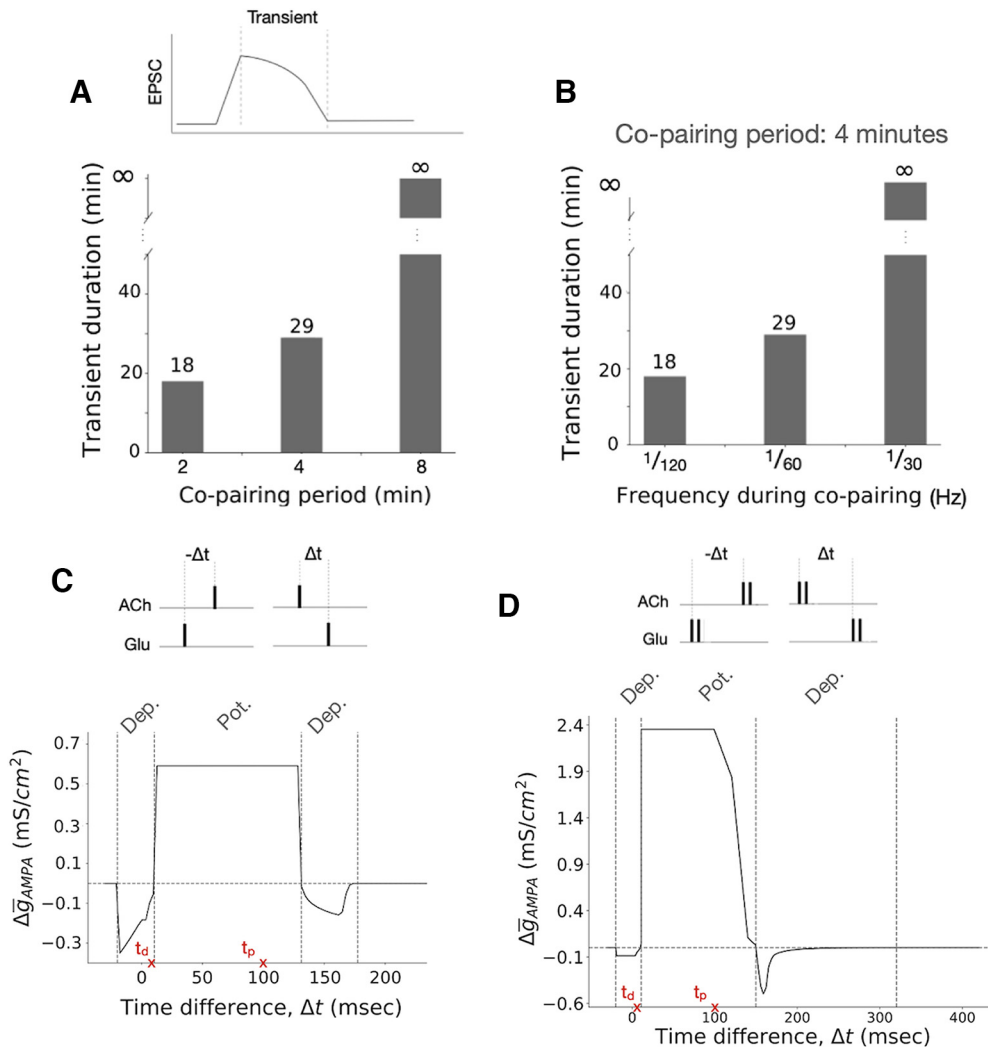First, we set out to study the cholinergic mechanisms by which activation of $\alpha7$ nAChRs on OLM$\alpha2$ neurons

Figure 3. Copairing temporal parameters determines the duration and polarity of synaptic plasticity: relative timing among cholinergic and glutamatergic stimulation, the extent of the copairing period, and the frequency of stimulation (model results). **A**, Synaptic strength transient duration is proportional to the extent of the pairing period. Here, the transient duration is defined as the time it takes the EPSC to go back to baseline after copairing is over. The I-cell and E_D receive a pulse of glutamate per minute. During the copairing period, the O-cell receives a pulse of ACh per minute, 100 ms before the glutamate pulses. **B**, Synaptic strength transient duration is proportional to the ACh and glutamate pulses frequency during the copairing period. Before and after the copairing period, the I-cell and E_D receive a pulse of glutamate per minute. During the copairing period (4 min), the frequency changes to 1/20, 1/60, or 1/30 s, and the O-cell receives a pulse of ACh 100 ms before the glutamate pulses with the same frequency. **C**, Relative pairing timing of single pulses provides a window of opportunity for plasticity. If glutamatergic inputs are administered within $10.4\,\text{ms} < \Delta t < 131.1\,\text{ms}$, the E_D excitatory synapse is potentiated. If glutamatergic inputs are administered within $-19.9\,\text{ms} < \Delta t < 10.4\,\text{ms}$ or $10.4\,\text{ms} < \Delta t < 131.1\,\text{ms}$, depression is induced. The change in the AMPAR conductance $\Delta \bar{g}_{AMPA}$ is measured 60 ms after one pairing. The relative time between cholinergic and glutamatergic activation of the network determines how efficiently the O-cells suppress spiking of the I-cells, as shown in Extended Data Figure 3-1. If noise is added to the membrane potential of E_D, the window of depression and potentiation is not as well defined, as shown in Extended Data Figure 3-2. **D**, Pairing multiple pulses of glutamate and ACh can change the window of opportunity for plasticity. Two pulses of glutamate and ACh with a frequency of 2 Hz are paired. If glutamatergic inputs arrive within $-19.9\,\text{ms} < \Delta t < 10.9\,\text{ms}$ or $149.9\,\text{ms} < \Delta t < 320\,\text{ms}$ of the cholinergic inputs, depression is induced. If glutamatergic inputs are administered within $10.9\,\text{ms} < \Delta t < 149.9\,\text{ms}$, the E_D excitatory synapse is potentiated. The change in the AMPAR conductance $\Delta \bar{g}_{AMPA}$ is measured 60 ms after one pairing. The pairing times of cholinergic and SC inputs found by Gu and Yakel (2011) to induce short-term depression and long-term potentiation at the SC–CA1 synapse (indicated with the red cross) are within our range of depression and potentiation.

facilitates the potentiation of SC–CA1 synapses. We designed a biophysical model to reproduce the experimental results reported in the study by Gu et al. (2020; Fig. 2A,C) using the minimal network scheme presented in Figure 2B.

In our model, similar to what was reported in the study by Gu et al. (2020), repeated coactivation of cholinergic and glutamatergic inputs potentiates the SC–CA1 synapse (Fig. 2D). The longer the coactivation period, the longer lasting are these changes.
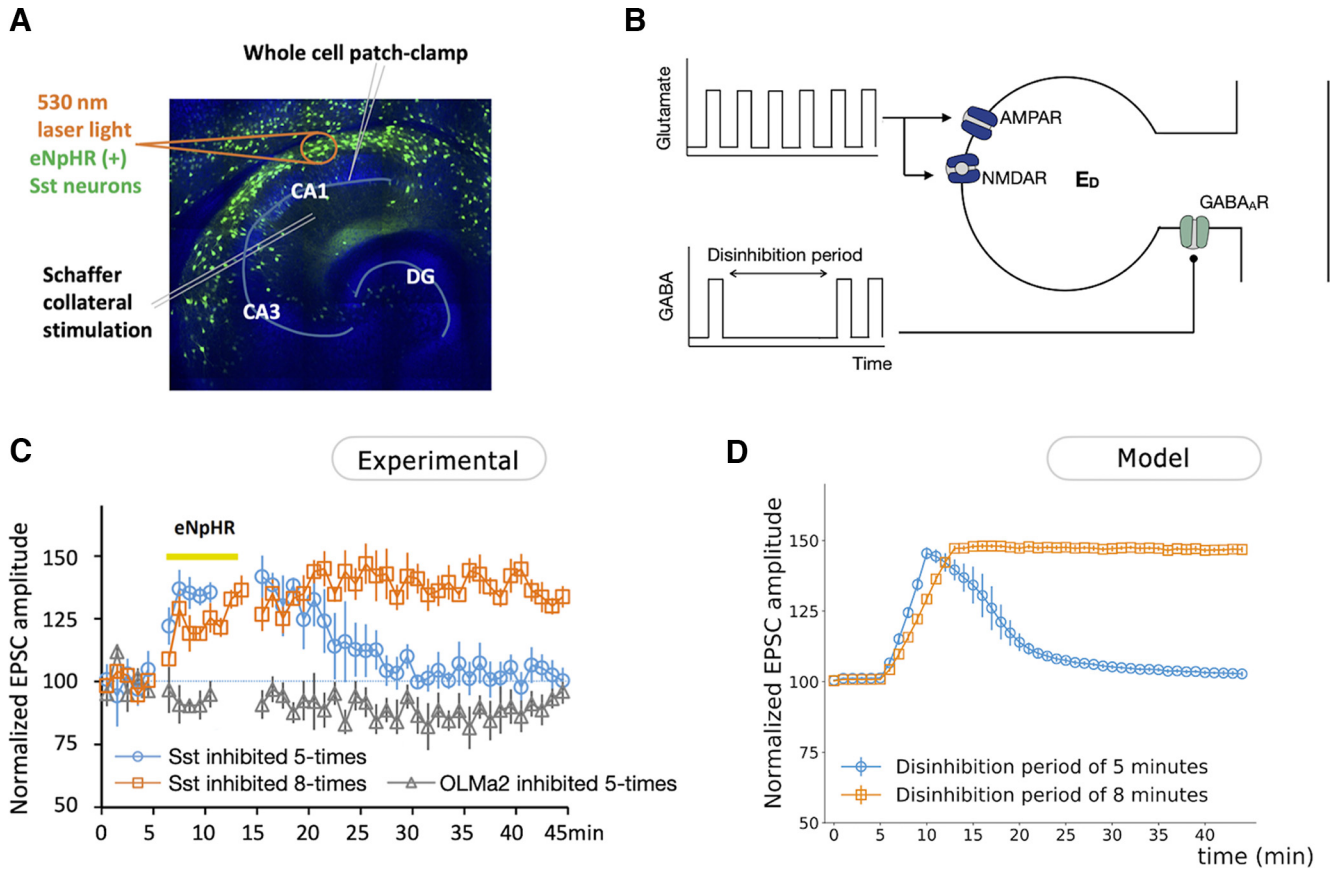
Figure 4. Disinhibition of CA1 pyramidal cell facilitates the induction of hippocampal synaptic plasticity. **A**, Scheme of *in vitro* induction of hippocampal synaptic plasticity through concurrent Sst inhibition. EPSCs were recorded from CA1 pyramidal neurons. Sst neurons were inhibited via eNpHR that was specifically expressed in Sst-positive neurons. The SC pathway was activated by a stimulating electrode. **B**, Schematic representation of a CA1 pyramidal neuron dendritic compartment E_D with postsynaptic $GABA_A$, AMPA, and NMDA receptors used to study the disinhibitory mechanisms for induction of plasticity at the SC–CA1 excitatory synapse. The dendritic compartment of the pyramidal cell receives one pulse of both glutamate and GABA per minute, except during the disinhibition period, where it only receives pulses of glutamate. The GABA pulse, presumably from the I-cell, is described by a square function with similar amplitude and duration as the glutamate pulse (see Materials and Methods; Extended Data Figs. 4-1, 4-2, justification). Glutamate binds to the excitatory AMPA and NMDA receptors, while GABA binds to the inhibitory $GABA_A$ receptor. The synaptic currents and membrane potential of E_D when a pulse of glutamate is paired (or not) with a pulse of GABA are shown in Extended Data Figure 4-3. **C**, Experimental measurements showing the effects of inhibition of Sst and OLMα2 interneurons in s.o. on SC-evoked EPSCs ($n = 5$ slices for each group). Inhibition of Sst interneurons from $t = 5$ min to $t = 10$ min enhanced the SC-evoked EPSC amplitude of the CA1 pyramidal cell, followed by a return to the baseline after the inhibition period (blue line). Inhibition of Sst interneurons from $t = 5$ min to $t = 13$ min increased SC-evoked amplitude EPSCs, which remained potentiated after the inhibition period (orange line). **D**, Numerical simulation of normalized EPSCs of E_D for a disinhibition period of 5 min (from $t = 5$ min to $t = 10$ min) and 8 min (from $t = 5$ min to $t = 13$ min). Normalization of the results was calculated according with the expression $(100 + (EPSC – EPSC_{min}) \cdot (150–100))/(EPSC_{max} – EPSC_{min})$.

From Figure 2D, we see that during the copairing period (from $t = 10$ min to $t = 18$ min), the EPSC is increased. This increase in our model is maintained for an extended period after the copairing period is over (black line), matching experimental results. We also see that GABA release from the I-cells, GABA$_I$, decreases significantly (Fig. 2D, inset). Before the copairing period, glutamatergic inputs activate the I-cell. This results in the inhibition of the pyramidal cell dendritic compartment E_D, which shows an SC-evoked depolarization immediately followed by hyperpolarization of its membrane potential. During the copairing period, activation of α7 nAChRs 100 ms before SC stimulation results in a flux of calcium into the OLM cell

that will initiate CICR from internal stores exerting a positive feedback. The increase in intracellular calcium concentration induces the release of GABA, as described by Equation 16. GABAergic inputs from the OLM cell disable the SC-evoked activation of the I-cell. As a result, E_D does not receive GABAergic inputs (Extended Data Fig. 2-1).

If we reduce the maximal conductance of the α7 nAChR, $\bar{g}_{\alpha7}$ from 3 to 1.7 nS as an approximation of the effect of α7 knockout, copairing no longer potentiates the EPSC of E_D (Fig. 2D, orange line). These observations are in accordance with experimental results showing that this form of EPSC boost was abolished by knockout of the α7 nAChR in OLMα2 interneurons (Fig. 2C).

Table 3: Parameter values for calcium dynamics and synaptic plasticity

Parameter	Value	Reference
σ	0.0040 ms^{-1}	Materials and Methods
P_1	1.5e-6	Shouval et al. (2002)
P_2	$P_1 \times 10^{-4}$	Shouval et al. (2002)
P_3	13	Shouval et al. (2002)
P_4	1	Shouval et al. (2002)
$\theta_\uparrow$	0.34 μM	Materials and Methods
$\theta_\downarrow$	0.31 μM	Materials and Methods
$\gamma_\uparrow$	0.0687,* 0.0699[†] nS/ms	Materials and Methods
$\gamma_\downarrow$	0.0375 nS/ms	Materials and Methods
α	0.1	Burnashev et al. (1995)
ξ	0.006,* 0.045[†] μM/(ms/pA)	Sabatini et al. (2002)
τ_{Ca}	12 ms	Sabatini et al. (2002)
ξ'	2.1×10^{-6} mM/(ms pA)	Materials and Methods
α'	0.05	Vernino et al. (1994)
τ	10 ms	Materials and Methods
k_d	2×10^{-4} mM	Materials and Methods

*Values used to reproduce Figures 2 and 3.
[†]Values used to reproduce the remaining figures.

We then examined how the key parameters of the co-pairing protocol influence the plasticity of the SC–CA1 EPSCs. According to our model, the duration of the co-pairing period, the relative time between the cholinergic and glutamatergic inputs, as well as their frequency during the copairing period can modulate the efficiency and direction of plasticity. Our simulations show that the longer the copairing period, the longer it takes the EPSCs to return to the baseline value once the copairing period is over (Figs. 2D,F, 3A). We observe a positive relationship between the frequency of the glutamatergic and cholinergic inputs during a fixed period of paring protocol and the potentiation transient duration (Fig. 3B). Interestingly, our simulations suggested that while changing the copairing period and the frequency of stimulation modulates the efficiency of the induction of potentiation, it does not change the direction of plasticity. Only when varying the relative time between the ACh and glutamate pulses could we induce a change in the plasticity direction. For single-pulse pairing, potentiation will be induced if the glutamatergic inputs arrive at I and E_D within $10.4 < \Delta t < 131.1$ ms following the ACh pulse. If $-19.9 < \Delta t < 10.4$ ms or $131.1 < \Delta t < 177.4$ ms, depression is induced (Fig. 3C). If we pair doublets of glutamate and ACh with a frequency of 2 Hz instead of single pulses, the potentiation window is $10.9 < \Delta t < 149.9$ ms, while the depression window is $-19.9 < \Delta t < 10.9$ ms and $149.9 < \Delta t < 320$ ms (Fig. 3D). In both cases, the potentiation and depression window are well defined. These results agree with experimental findings by Gu and Yakel (2011) showing that the activation of cholinergic inputs 100 and 10 ms before SC stimulation induced SC to CA1 long-term potentiation and short-term depression, respectively.

In the simulations performed to reproduce Figure 3, C and D, we do not consider noisy membrane potentials. As a result, we obtain sharp transition between the regions of depression and potentiation—the timing at which GABA$_O$ is released from the O-cell finely tunes the number of spikes emitted by the I-cell. As we show in Extended Data

Figure 3-2, adding a noisy background induces spontaneous spiking of the O-cells and I-cells, which results in smoother transitions.

Disinhibition of the CA1 pyramidal cell dendritic compartment enables potentiation of the SC–CA1 synaptic transmission

Our model shows a decrease in GABA release from I-cells during the copairing period (Fig. 2D, inset) that results in disinhibition of the E_D. To study the role of this disinhibition in the potentiation of the SC–CA1 excitatory synapse, we used a model of E_D submitted to a pulse of glutamate followed by a pulse of GABA, except during a disinhibition period when it only receives pulses of glutamate (Fig. 4B, scheme). This corresponds to experiments where we paired, *in vitro*, the inhibition of Sst interneurons (analogous to the I-cells in the model) with SC stimulation that provides the glutamatergic inputs (Fig. 4A).

We would like to note that, according to our model, the rise and decay time of GABA concentration release that results from the spiking of the I-cells is almost instantaneous (Extended Data Fig. 4-1). Therefore, in this section, the GABAergic inputs into E_D are modeled as square pulses. For simplicity, both glutamate and GABA release pulses are modeled as square pulses with a duration of 1 ms and 1 mm of amplitude. It is important to note that pulses with amplitudes and durations different from the ones considered here would reproduce the same results, as long as the duration and amplitude of glutamate and GABA match each other (Extended Data Fig. 4-2A). E_D receives one pulse of glutamate per minute, followed by a pulse of GABA 2 ms after, except during a disinhibition period when it only receives pulses of glutamate. We note that this simulated stimulation and pairing choice directly follows the experimental protocol (see Materials and Methods).

In our model simulations, we observe that before the disinhibition period, there were no changes in the simulated EPSC amplitude of E_D. During the disinhibition period, the EPSC amplitude increases, and the longer the disinhibition period lasts, the longer these changes last. More specifically, for a disinhibition period of 5 min, the EPSC returns to baseline once the disinhibition period is over. For a longer disinhibition period of 8 min, the EPSC remains potentiated long after the disinhibition period is over (Fig. 4D). These results hold for different values of the plasticity parameters (Extended Data Fig. 4-2B). After 5 min of E_D disinhibition, the EPSC amplitude was increased from 169.40 to 285.34 pA. After 8 min of disinhibition, the EPSC amplitude increased to 361.33 pA. This is in accordance with experimental results, where inhibition of Sst interneurons projecting to CA1 pyramidal cells was paired with SC stimulation for a short and long period (Fig. 4C). Inhibition of Sst interneurons via eNpHR resulted in increased SC–CA1 EPSC amplitude not only during the Sst inhibition but also after the end of Sst inhibition. The EPSC enhancement after the Sst inhibition lasted ~10 min after 5 min of Sst inhibition and >30 min after 8 min of Sst inhibition. After 5 min of Sst inhibition, the EPSC amplitude was significantly increased at 5 min

after the end of Sst inhibition (31.8% increase compared with baseline, $p = 0.0003$) but returned to baseline at 30 min after Sst inhibition (2.8% increase compared with baseline, $p = 0.79$). After 8 min of Sst inhibition, the EPSC amplitude was significantly increased at both 5 min after the end of Sst inhibition (37.3% increase compared with baseline, $p < 0.0001$) and 30 min after Sst inhibition (32.5% increase compared with baseline, $p < 0.0001$). Experiments showed that the inhibition of OLMα2 interneurons via eNpHR did not change the amplitude of SC–CA1 EPSC, indicating that the Sst interneurons inducing potentiation do not include OLM (Fig. 4C, gray line).

AMPARs are known to play an important role in regulating and expressing synaptic plasticity in the hippocampus (Barria et al., 1997). From Figure 5, we see that there is an increase of $\bar{g}_{AMPA}$ during the disinhibition period. The longer the disinhibition period, the more significant the increase. For a disinhibition period of 5 min, there is an increase of $\bar{g}_{AMPA}$ from 4 to 6.9 nS during disinhibition. Afterward, $\bar{g}_{AMPA}$ gradually goes back to its baseline value (Fig. 5A). For a disinhibition period of 8 min, $\bar{g}_{AMPA}$ increases from 4 to 8.83 nS. When the disinhibition period is over, $\bar{g}_{AMPA}$ remains potentiated (Fig. 5B). It is important to note that without regular synaptic stimulation, $\bar{g}_{AMPA}$ decays back to its resting value after the disinhibition period (i.e., $\bar{g}_{AMPA}$ has only one stable fixed point and is not bistable).

In this study, we focused on a calcium-based synaptic plasticity model to describe changes in the excitatory SC–CA1 synapse. To gain a more detailed understanding on how the evolution of the calcium levels relate to the changes in the synaptic strengths, we can examine the calcium dynamics before, during, and after the disinhibition period.

Figure 5, C and D, shows that the calcium concentration increases significantly during the disinhibition period, crossing the potentiation onset $\theta_\uparrow$ with a significant margin. Immediately after the end of the disinhibition period, the calcium levels decrease, yet they remain above $\theta_\uparrow$. We can see a clear difference in calcium dynamics for the short and the long disinhibition periods. In the case of a short disinhibition period, each pairing of GABA and glutamate after the disinhibition period will elicit a calcium pulse with a smaller amplitude than the previous one. Eventually, at $t = 25$ min, the calcium concentration from the pairing is not enough to cross the potentiation onset $\theta_\uparrow$. By $t = 30$ min, calcium does not cross either the potentiation ($\theta_\uparrow$) or the depression onset ($\theta_\downarrow$), having a similar amplitude as before the disinhibition period. In the case of a long disinhibition period, each pairing performed after the disinhibition period evokes a calcium pulse with a constant amplitude. In other words, long disinhibition periods ensure that the consequent pairings yield calcium responses that do not drop below the onset thresholds.

To better visualize the synaptic and calcium dynamics immediately after the disinhibition period in both cases, we plot the trajectory of the system in the Ca-$\bar{g}_{AMPA}$ plane. We do so for $\bar{g}_{AMPA}(t_{init}) = 6.9$ nS and for $\bar{g}_{AMPA}(t_{init}) = 8.83$ nS, which are the values of $\bar{g}_{AMPA}$ at the end of the disinhibition period for the short and long disinhibition

durations (Fig. 5E). For $\bar{g}_{AMPA}(t_{init}) = 6.9$ nS, the calcium concentration crosses the potentiation onset $\theta_\uparrow$ (Ca$_{max} = 0.353$ μM), but there is a decrease of $_< \bar{g}_{AMPA}$ from 6.9 to 6.8 nS. For $\bar{g}_{AMPA}(t_{init}) = 8.83$ nS, the calcium concentration crosses $\theta_\uparrow$ to a larger extent (Ca$_{max} = 0.389$ μM) and there is an increase of $\bar{g}_{AMPA}$ from 8.83 to 8.92 nS. These results suggest that it is necessary but not sufficient for calcium concentration to cross the potentiation onset to induce potentiation. To verify this, we looked at changes in maximal conductance of the postsynaptic AMPAR ($\Delta\bar{g}_{AMPA}$), as a function of the amplitude of the intracellular calcium (Ca$_{max}$). From Figure 5F, we see that as Ca$_{max}$ increases we only start to have potentiation ($\Delta\bar{g}_{AMPA} > 0$) when Ca$_{max}$ crosses not the potentiation onset $\theta_\uparrow$, but a higher level, which we term as the potentiation threshold θ_{pot}, 0.36 μM.

We do note that the fixed potential threshold θ_{pot} is not an ideal indicator of potentiation, as it may need to be recalculated depending on a specific case of calcium dynamics timescales and/or the induction protocol. As seen in Figure 5E, the dynamics of calcium is important in the induction of plasticity. Therefore, changing these by, for example, changing the calcium decay rate, can alter the θ_{pot} by changing the time calcium spends in the depression/potentiation onset region. This kind of analysis can also fail to identify mechanisms of the induction of potentiation. As shown in Figure 6B, if we consider a second calcium source that becomes activated at $t = 80$ ms, neither of the two pulses of calcium generated crosses θ_{pot}; however, the synapse is potentiated. These examples suggest that it is not the peak calcium concentration that is a key indicator of potentiation, but a measure that is based on the total amount of calcium that exceeds the onset levels. We suggest that a better quantity that can be used more generally as an indicator of plasticity is the ratio between the integral of calcium when its concentration is above the potentiation onset $\theta_\uparrow$, which we will call the area of AMPAR insertion (Extended Data Fig. 6-1, orange area, Fig. 6, corresponding graphs) and the integral of calcium when its concentration is above the depression onset $\theta_\downarrow$ and below the potentiation onset $\theta_\uparrow$, the area of AMPAR removal (Extended Data Fig. 6-1, gray area, Fig. 6, corresponding graphs) weighted by the calcium-dependent learning rate η, which we named (A$_\uparrow$/A$_\downarrow$)$_w$ (for more details, see Materials and Methods). If this ratio is < 3.0, depression is induced in our model; if the ratio is > 3.0, potentiation is induced.

GABA amplitude and Glu–GABA pairing timing control membrane potential

Disinhibition of the pyramidal cell (i.e., reduction of GABAergic inputs), can facilitate the depolarization of the cell, which can control plasticity, as we have shown in the previous section. Therefore, we hypothesize that the amplitude of the GABA pulse, GABA$_{max}$, and the relative time between the glutamate and GABA pulses, $\Delta t_{(GABA-Glu)}$, can modulate plasticity. To explore this hypothesis, we pair glutamatergic inputs with GABAergic inputs into E$_D$. We vary the relative time between the inputs, $\Delta t_{(GABA-Glu)}$, and the amplitude of the GABAergic inputs, GABA$_{max}$, to
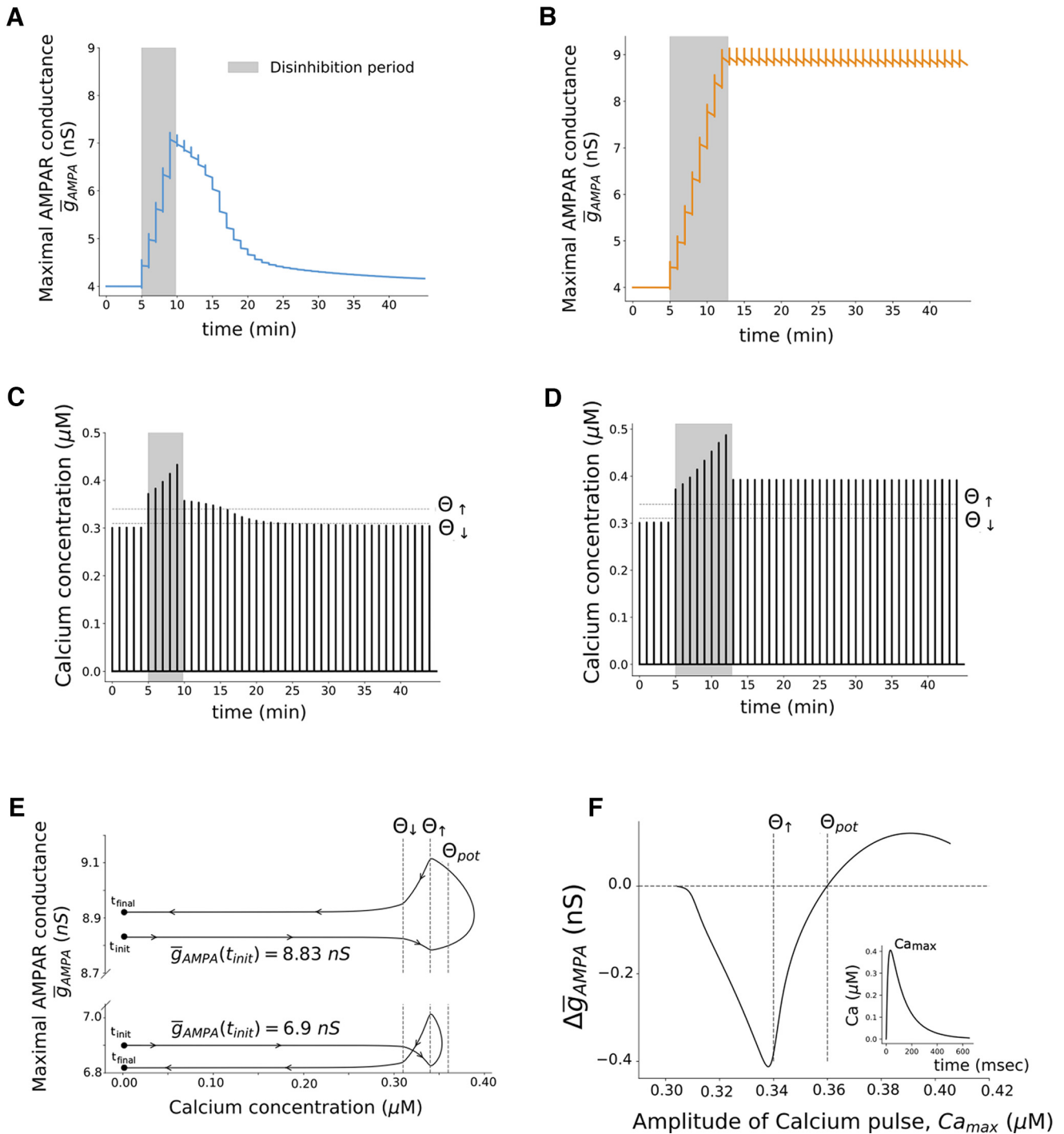
Figure 5. Calcium dynamic is key for the induction of synaptic plasticity. **A**, Time course of maximal AMPAR conductance, $\bar{g}_{AMPA}$, when the dendritic compartment is disinhibited for a short period (from $t = 5$ min to $t = 10$ min). The maximal AMPAR conductance increases from its initial value $\bar{g}_{AMPA} = 4$ nS to $\bar{g}_{AMPA} = 6.9$ nS during the disinhibition period (gray area). **B**, Time course of $\bar{g}_{AMPA}$ when the dendritic compartment is disinhibited for a long period (from $t = 5$ min to $t = 13$ min). It increases from $\bar{g}_{AMPA} = 4$ nS to $\bar{g}_{AMPA} = 8.83$ nS during the disinhibition period. Changes in the AMPAR conductance, $\bar{g}_{AMPA}$, are described by Equation 22. **C**, Time course of intracellular calcium concentration when E$_D$ is disinhibited for a short period (from $t = 5$ min to $t = 10$ min), where $\theta_{\downarrow}$ is the depression onset, and $\theta_{\uparrow}$ is the potentiation onset. **D**, Time course of intracellular calcium concentration when the dendritic compartment is disinhibited for a long period (from $t = 5$ min to $t = 13$ min). The calcium dynamics is described by Equation 25 (see Materials and Methods). **E**, Trajectories of the system in the $\bar{g}_{AMPA}$–Ca plane when a pulse of glutamate is paired with a pulse of GABA for $\bar{g}_{AMPA} = 6.9$ nS and $\bar{g}_{AMPA} = 8.83$ nS, where θ_{pot} is the potentiation threshold as defined in the Results section. **F**, Changes in the maximal AMPAR conductance, $\Delta\bar{g}_{AMPA}$, as a function of the amplitude of intracellular calcium pulse, Ca$_{max}$. Each point of the graph was obtained by submitting E$_D$ to a glutamate pulse for different initial values of $\bar{g}_{AMPA}$. This induced different depolarization levels and, consequently, different activation levels of NMDARs and calcium pulses of different amplitudes.
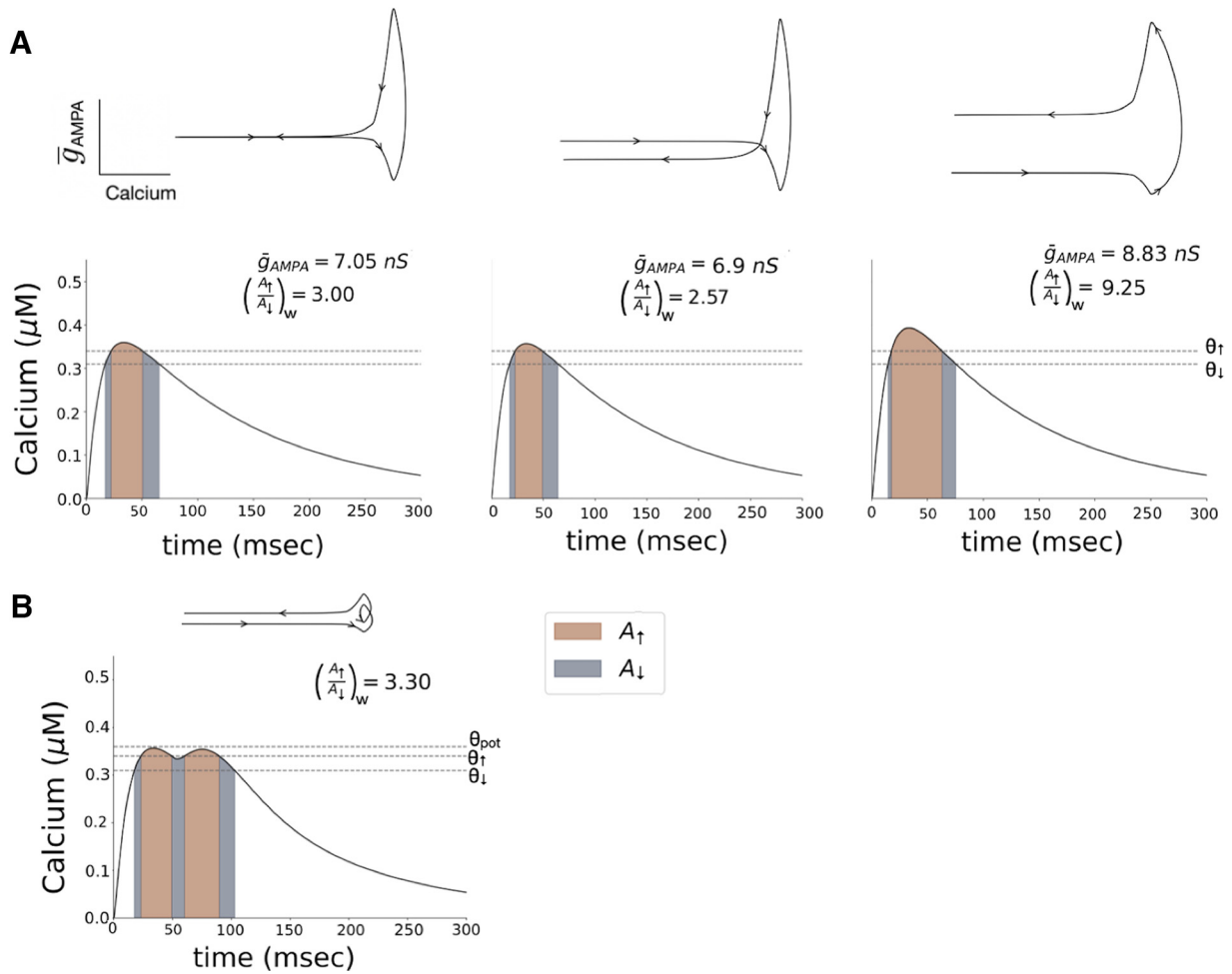
A

B

Figure 6. The weighted ratio $(A_\uparrow/A_\downarrow)_w$ can accurately be used as a predictor of induction of depression or potentiation. The depression and potentiation areas $A_\downarrow$ and $A_\uparrow$ are as defined in Extended Data Figure 6-1. **A**, Different values of $\bar{g}_{AMPA}$ evoke different levels of depolarization and, consequently, different intracellular calcium concentrations. For a weighted ratio between the calcium area of AMPAR insertion and removal at <3.00, depression is induced. For a value >3.00, potentiation is induced. **B**, By adding a second source of calcium that becomes activated at $t = 80$ ms, it is possible to have situations where the calcium never crosses the potentiation threshold θ_{pot} but potentiation is induced. The $(A_\uparrow/A_\downarrow)_w$ accurately identifies these cases as potentiation. In these numerical simulations, E_D receives a pulse of glutamate followed by a pulse of GABA 2 ms after, each with an amplitude of 1 mM and a duration of 1 ms.

measure changes induced in $\bar{g}_{AMPA}$. Simulations were repeated for different values of $\bar{g}_{AMPA}$ to understand why pulses of glutamate and GABA with the same characteristics (same amplitude and same duration) have different outcomes when administered after the short or long disinhibition periods. Simulations were performed with three initial values of $\bar{g}_{AMPA}$: $\bar{g}_{AMPA} = 4$ nS, $\bar{g}_{AMPA} = 6.9$ nS, and $\bar{g}_{AMPA} = 8.83$ nS. We identified well defined regions of potentiation and depression in the $\Delta t_{(GABA-Glu)}$–$GABA_{max}$ parameter space (Fig. 7). We also saw that the regions change with the value of $\bar{g}_{AMPA}$. More specifically, the depression region moves toward the right of the plot as $\bar{g}_{AMPA}$ increases. In other words, as $\bar{g}_{AMPA}$ increases, the GABAergic inputs need to arrive with a longer delay relative to the glutamatergic inputs to induce depression. It is important to note that the level of potentiation or depression induced also changes as we increase $\bar{g}_{AMPA}$. Generally, the magnitude of potentiation decreases, and

the magnitude of depression increases. This is because the system saturates as $\bar{g}_{AMPA}$ increases (i.e., $\bar{g}_{AMPA}$ cannot increase indefinitely). This is a restriction imposed by the model. These results suggest that the same induction protocol may induce either potentiation or depression more or less efficiently, depending on the current phosphorylation state of the AMPA receptors (i.e., $\bar{g}_{AMPA}$), and on the decrease of GABA during disinhibition. In other words, the net effect of a pairing protocol is state dependent.

Model predictions and implications

Results of model simulations and analysis make several testable predictions. First, while experiments so far have not identified precisely the exact type of s.o. interneurons that provide the feedforward inhibition to the CA1 pyramidal cell, our model predicts that it should be
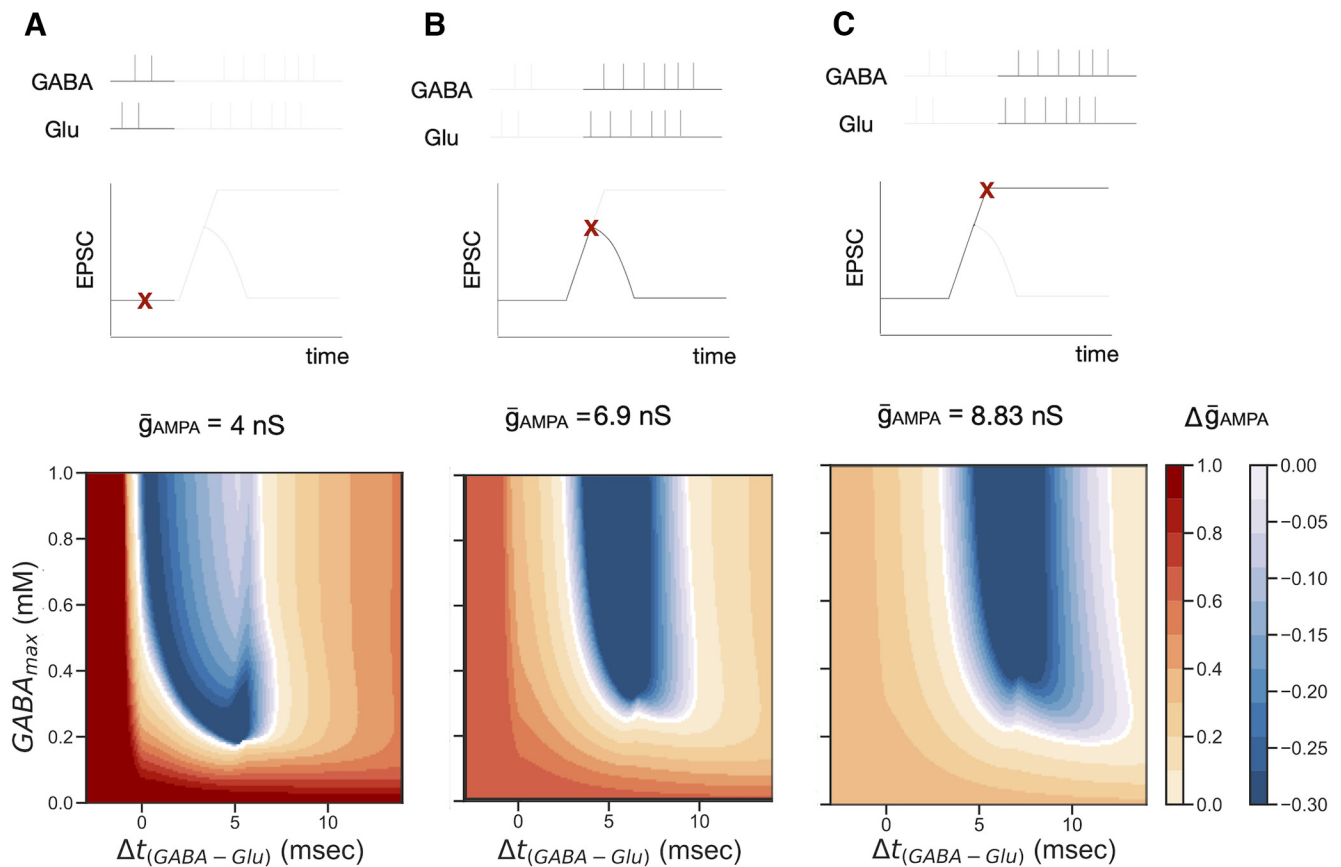
Figure 7. Amplitude of GABA pulse, GABA$_{max}$, and relative time between GABA and glutamate pulses, $\Delta t_{(GABA-Glu)}$, control the direction and efficiency of the induction of synaptic plasticity. ***A***, Depression and potentiation regions for $\bar{g}_{AMPA}$ = 4 nS. This is the maximal conductance value of the AMPAR used in our simulations before the disinhibition period starts. ***B***, Depression and potentiation regions for $\bar{g}_{AMPA}$ = 6.9 nS, which represents the state of phosphorylation of the AMPAR at the end of the short disinhibition period. ***C***, Depression and potentiation regions for $\bar{g}_{AMPA}$ = 8.83 nS, which is the state of phosphorylation of the AMPAR at the end of the long disinhibition period. For each plot in ***A***, ***B***, and ***C***, we pair one pulse of glutamate (with a concentration of 1 mM and 1 ms of duration) with one pulse of GABA with a duration of 1 ms and varying concentrations and initial time, and measure the resultant change in $\bar{g}_{AMPA}$ for each case.

an interneuron type with fast dynamics (i.e., with dynamics comparable to the pyramidal cells). More specifically, we expect that EPSC on the hippocampal parvalbumin (PV)-positive interneurons in the stratum radiatum would decrease during cholinergic pairing because of the inhibition provided by the OLM neurons. Consequently, GABA$_A$-mediated IPSCs on the proximal dendrites of CA1 pyramidal cells would also decrease.

In this work (both in modeling and experimentally), modulation of the OLM cells is because of cholinergic activation of $\alpha 7$ nAChRs. Our model more specifically suggests that the GABA release by the OLM cells is regulated by activating $\alpha 7$ nACh receptors, without necessarily altering the OLM firing. However, GABA release can also be controlled by the depolarization of the OLM cells and/or by modulation of their spiking activity by somatic nAChRs.

Our model predicts a relationship between the relative timing of the septal and hippocampal stimulus pairing and the synaptic plasticity direction at the SC–PYR synapse. According to our simulations, increasing the frequency of septal and hippocampal paired stimulation can induce

plasticity more efficiently (i.e., fewer pairings would be required to induce LTP). At the same time, we predict that changing the relative time between septal and hippocampal activation can induce long-term depression instead of LTP.

Finally, our modeling results suggest that for the plasticity to be induced, the excitatory NMDA and AMPA receptors and the inhibitory GABA$_A$ receptors should be located sufficiently proximal to each other in the pyramidal dendritic compartment.

Discussion

This work set out to explain how nicotinic cholinergic modulation of hippocampal OLM interneurons paired with hippocampal stimulation can potentiate CA1 pyramidal cell EPSC responses. Our modeling results suggest that copairing cholinergic activation of $\alpha 7$ nAChRs on the OLM interneurons results in disinhibition of CA1 pyramidal cells. We also show by mathematical analysis how synaptic plasticity is controlled by the disinhibition of the postsynaptic pyramidal membrane through a disynaptic

GABAergic circuit. To our knowledge, this is the first report to reveal how repeated disinhibition can directly induce short-term or long-term potentiation, depending on the duration of the disinhibition period (both experimentally and computationally). It is also the first computational study that explicitly shows how cholinergic action on OLM interneurons can directly induce SC–CA1 plasticity through disinhibition.

OLM cells are a major class of GABAergic interneurons located in the stratum oriens hippocampal layer that inhibit pyramidal cells dendritic compartment located in the stratum lacunusom-moleculare layer, reducing the strength of EC inputs. OLM cells also target bistratified interneurons, expressing PV and somatostatin (Sst), that receive feedforward excitatory inputs from the Schaffer collaterals (Müller and Remy, 2014). Recent findings show that activation of OLM cells can facilitate LTP in the SC–CA1 pathway, likely by inhibiting s.r. interneurons that synapse on the same dendritic compartment as the SC, counteracting SC feedforward inhibition (Leão et al., 2012). We found that repeated pairing of cholinergic inputs with hippocampal stimulation can induce plasticity if the inputs are tightly timed. The time window for potentiation depends significantly on the dynamics of the O-cells and I-cells, and calcium dynamics. This agrees with experimental findings showing that activating cholinergic inputs to the hippocampus can directly induce different forms of synaptic plasticity depending on the input context of the hippocampus, with a timing precision in the millisecond range (McKay et al., 2007; Gu and Yakel, 2011). Our model also shows that the longer the copairing period and the higher the frequency of stimulation during the copairing period, the longer lasting is the potentiation of the synapse.

According to our model, the key mechanism behind paired cholinergic induction of synaptic plasticity is the disinhibition of the pyramidal cell dendritic compartment. Cholinergic activation of the O-cell synapses inhibits the fast-spiking I-cell that projects to the dendritic compartment E_D. The disinhibition of E_D paired with glutamatergic stimulation allows for the depolarization of the pyramidal dendritic compartment. This increases NMDAR activation and intracellular calcium concentration sufficient to upregulate postsynaptic AMPAR permeability and potentiate the excitatory synapse. Our model puts together all the elements to give the following sequence of events: SC stimulation results in the activation of CA1 fast-spiking interneurons, I, and the subsequent release of GABA. At the same time, it evokes an EPSP mediated by AMPAR on the CA1 pyramidal cell dendritic compartment, E_D. Since I and E_D have comparable dynamics, the EPSP is closely followed by a GABA$_A$-mediated IPSP. Because of slow kinetics and voltage dependence, at that time, the NMDAR receptors are not in the open state and there is no significant influx of calcium. When the SC inputs are tightly timed with cholinergic inputs acting on OLM interneurons, GABA release from I-cells is suppressed. The pyramidal cell membrane at (or sufficiently near to) the glutamatergic synapse can depolarize enough to relieve the Mg^{2+} block from the NMDA receptors, allowing calcium to permeate through the receptor channel (Fig. 8). Therefore, every time the pyramidal cell receives a glutamate pulse during the disinhibition period, the intracellular calcium concentration crosses the potentiation outset $\theta_\uparrow$, and $\bar{g}_{AMPA}$ increases.

Downregulation of the GABAergic signaling during disinhibition leads to increased NMDAR activation. We see that when we reduced GABA concentration, glutamatergic activation of E_D results in postsynaptic NMDA currents with 7.90 pA of amplitude—with depolarization of -58.25 mV, as opposed to the 6.75 pA that results from the pairing of glutamate and GABA inputs—with depolarization of -63.56 mV (Extended Data Fig. 4-3). Because of the high calcium permeability of receptor, there is an elevation in intracellular calcium concentration large enough to initiate molecular mechanisms that result in the insertion/phosphorylation of the AMPAR. In our model, this translates into an increase in the AMPAR maximal conductance $\bar{g}_{AMPA}$. Moderate calcium concentrations, on the other hand, result in the removal of AMPARs. Because changes in calcium concentration are not instantaneous, the potentiation/depression of the synapse results from a balance between the insertion/removal of AMPARs during the period in which Ca concentration is above the potentiation/depression threshold. During disinhibition, this balance is positive and there is a total increase in $\bar{g}_{AMPA}$.

The more times we pair disinhibition with SC stimulation (i.e., the longer the disinhibition period), the higher the value of $\bar{g}_{AMPA}$ by the end of the disinhibition period. After the disinhibition period, if the increase of $\bar{g}_{AMPA}$ was large enough, the calcium resultant from glutamatergic and GABAergic stimulation is such that there is a balance between potentiation and depression close to zero. That is, $\bar{g}_{AMPA}$ stabilizes by oscillating around the value of $\bar{g}_{AMPA}$ at the end of the disinhibition period (8.83 nS). Therefore, the synapse remains potentiated long after the disinhibition period is over. If there is no stimulation after the disinhibition period, $\bar{g}_{AMPA}$ slowly decays to its initial value (i.e., its value before the disinhibition period). Supposing that the increase of the AMPAR permeability is high enough, the potentiation of the excitatory synapse is maintained when the disinhibition period is over through repeated stimulation of the SC that keeps a balance between the downregulation and upregulation of the AMPARs. This is in accordance with experimental results that show repeated pairing of the inhibition of Sst interneurons (that were not OLM) that target the CA1 pyramidal cell with SC stimulation can induce plasticity.

We asked how the results of our simulations depend on the parameters chosen. We found that our model remains robust to changes of parameters as long as we maintain the same ratio of insertion/removal of AMPARs. Thus, for example, for different values of the $\gamma_\uparrow$, there is (at least) a pair of $\gamma_\downarrow$ for which our results remain the same (Extended Data Fig. 4-2B).

In our modeling study, we strived to ensure that parameters for which physiological ranges can be identified agree with these ranges. At the same time, there were a number of them that could not be constrained directly, and we chose to optimize them to obtain model responses that
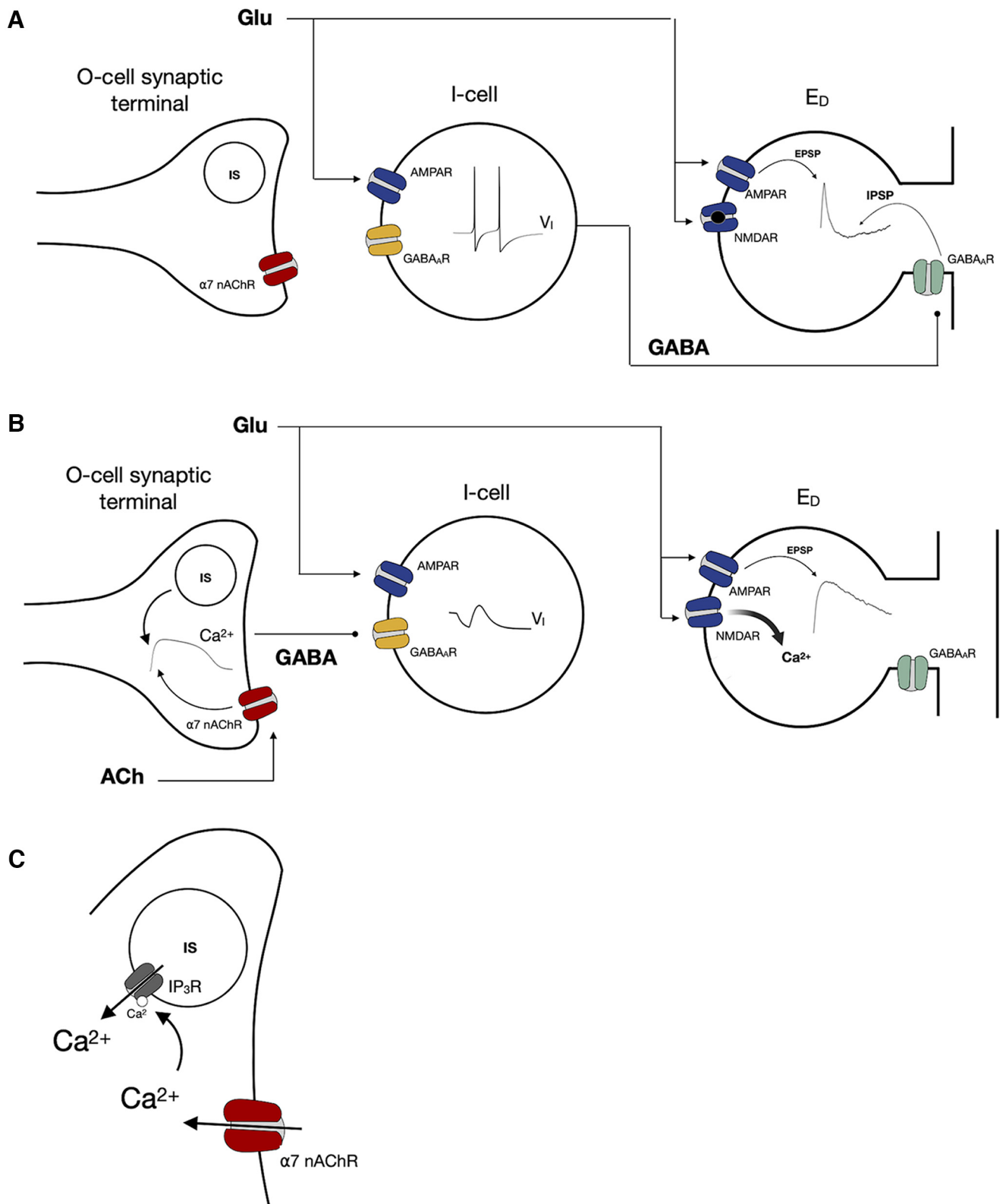
Figure 8. Scheme of the cholinergic and disinhibitory mechanisms that drive SC–CA1 potentiation. ***A***, Glutamatergic activation of I-cells lead to spiking activity and consequent GABA release. Subsequently, glutamate inputs acting on E_D evoke an EPSP mediated by AMPAR immediately followed by an IPSP-mediated GABA acting on $GABA_A$ receptors. ***B***, Cholinergic activation of $\alpha 7$ nAChR on OLM interneuron initiates a CICR process mediated by calcium internal stores (IS). This result in GABA release that inhibits the I-cell. The dendritic compartment does not receive GABAergic inhibition. The dendritic compartment can depolarize enough—and remain depolarized for long enough—to relieve Mg^{2+} block from NMDA receptors,

continued

allowing calcium to permeate through the receptor channel. **C**, CICR mechanism. The entry of calcium through α7 nAChRs induces calcium release form internal stores by activating IP$_3$ receptors.

qualitatively agreed with our data. For example, the calcium amplitude in our model is of the same order of magnitude as measured in the dendritic spines in the studies by Sabatini et al. (2002) and Rubin et al. (2005). While we do see that the optimized Ca$_p$ parameter is below the calcium resting value, we consider that calcium concentration decays to zero, similar to what is done in the studies by Graupner and Brunel (2005, 2012), Higgins et al. (2014), Rubin et al. (2005), and Shouval et al. (2002). Despite not being an exhaustively detailed description of what happens in the dendritic spine, changing the resting value of the calcium does not alter our results as long as it is below the depression threshold. Concerning the K$_{(Ca)p}$ parameter, it determines the steepness of the GABA$_O$(Ca) function. The vesicular release of neurotransmitter has a steep dependence on the intracellular calcium concentration Schneggenburger and Forsythe (2006). Thus, we believe it to be appropriate to consider a steep relationship between the intracellular calcium and the concentration of GABA available for binding, and that these two parameters are examples for functionally optimized values.

It is worth noting that the parity of the synaptic plasticity induced depends on the value of maximal conductance of the postsynaptic AMPAR, $\bar{g}_{AMPA}$, as shown in Figure 7. Therefore, our model indicates that future changes in synaptic strength depend on previous plasticity events and how these changed $\bar{g}_{AMPA}$. This explains why, after the disinhibition period, glutamate–GABA pulse pairs with the same characteristics will induce different results when the disinhibition period was short or long.

Earlier studies pointed out that reduced inhibition (disinhibition) can facilitate LTP induction under various conditions (Wigström and Gustafsson, 1985; Ormond and Woodin, 2009; Yang et al., 2016). Our results show that repeated temporally precise concurrent disinhibition can directly induce SC to CA1 LTP, providing a novel mechanism for inhibitory interneurons to modify glutamatergic synaptic plasticity directly. This expands the original spike timing-dependent plasticity that concerns the concurrent activation of two excitatory pathways to include the interneuron network. Furthermore, our modeling work implies that GABAergic neurotransmission should control the local pyramidal voltage in the vicinity of the glutamatergic synapses, thereby the inhibitory synapses critically modulate excitatory transmission and the induction of plasticity at excitatory synapses. This points toward the importance of dendritic GABA and glutamate colocation in shaping local plasticity rules. Our work also suggests a cholinergic mechanism for controlling GABA release at the pyramidal dendrites and the subsequent potentiation of excitatory synapses, unraveling the intricate interplay of the hierarchal inhibitory circuitry and cholinergic neuromodulation as a mechanism for hippocampal plasticity.

Previous work by Gu et al. (2017) showed that copaired activation of the cholinergic input pathway from the septum to the hippocampus with stimulation of the Schaffer collateral pathway could readily induce theta oscillations in a coculture septal–hippocampal–entorhinal preparation. Moreover, after performing copaired activation several times, not only was the SC–PYR synapse potentiated, but it became easier to evoke the theta rhythm in the preparation (one pulse stimulus of the SC is sufficient to generate theta oscillations in the circuit with the same characteristics as before; Gu and Yakel, 2017; Gu et al., 2017). Therefore, induction of hippocampal plasticity, particularly potentiation of the CA1 EPSPs, appears to facilitate the generation of the theta rhythm. Moreover, previous studies directly linked OLMα2 interneurons to theta oscillations (Rotstein, et al., 2005; Mikulovic, et al., 2018) and suggest that OLM cells can regulate the robustness of the hippocampal theta rhythm (Chatzikalymniou and Skinner, 2018). Thus, we may speculate that the action of ACh on the α7 nAChRs at the OLMα2 neurons potentiates the SC–CA1 synapses to close the critical link in the synaptic chain of events, enabling recurrent reverberation excitation in the hippocampal–entorhinal theta-generating circuit. Understanding the mechanisms underlying the induction of hippocampal plasticity by this copairing mechanism will allow future studies of how changes on the synaptic level can propagate to the network level and change the mechanisms of theta generation.

Our results are also relevant to understanding the neural circuit origins of pathologic conditions and uncovering potential targets for therapeutic intervention in disorders linked to memory deficits. For example, the hippocampus is one of the earliest brain structures to develop neurodegenerative changes in AD (Arriagada et al., 1992). Furthermore, numerous studies suggest that cognitive deficits in AD, such as memory impairment, are caused in part by the dysfunction of cholinergic action on hippocampal GABAergic interneurons (Schmid, et al., 2016; Haam and Yakel, 2017). Here, we have shown that a decrease in the conductance of cholinergic α7 nAChRs on OLM interneurons caused the impairment of induction of hippocampal synaptic plasticity.

Model caveats

As with any modeling studies we had to compromise between a realistic description of the neural networks and the simplicity of the model that allows for computational analysis. While some of the aspects could be performed using simplified integrate-and-fire neuron models, we felt that multiple aspects focused on biophysical mechanisms (e.g., the ability of the cholinergic activation of OLM cells to suppress spiking of fast-spiking interneurons in a tightly timed manner). The simplified one-compartment biophysical model used in this study allows us to analyze how detailed biophysical mechanisms, such as CICR and the dynamics of neurotransmitter release, control cholinergic induction of plasticity, while maintaining the simplicity and flexibility

necessary to carry out computational analysis and study similar mechanisms in other neural networks.

The assumptions and ad hoc simplifications made in this study introduce some limitations in the model. Namely, the description of the ACh pulse that, because of a lack of knowledge of the neurotransmitter profile in the synaptic cleft, is described as a square with 1 mM magnitude and a duration of 5 ms. We have shown that our results still hold up when considering different cholinergic profiles (Extended Data Fig. 2-3); however, a magnitude or duration considerably higher (lower) than what is considered here can lead to calcium concentrations that are too high (low). This can lead to nonphysiological calcium concentrations and, consequently, unrealistic GABA profile. In that case, one would have to consider a more detailed description of the CICR mechanism with calcium pumps on the internal stores and the membrane of the neuron. The same adjustment would be necessary if the resting calcium concentrations in the internal stores and intracellular medium induce a greater calcium flux.

References

Ali A, Deuchars J, Pawelzik H, Thomson AM (1998) CA1 pyramidal to basket and bistratified cell EPSPs: dual intracellular recordings in rat hippocampal slices. J Physiol 507:201–217.

Alkondon M, Pereira E, Barbosa C, Albuquerque E (1997) Neuronal nicotinic acetylcholine receptor activation modulates gamma-aminobutyric acid release from CA1 neurons of rat hippocampal slices. J Pharmacol Exp Ther 283:1396–1411.

Andrásfalvy BK, Smith MA, Borchardt T, Sprengel R, Magee JC (2003) Impaired regulation of synaptic strength in hippocampal neurons from GluR1-deficient mice. J Physiol 552:35–45.

Arriagada P, Growdon J, Hedley-Whyte E, Hyman B (1992) Neurofibrillary tangles but not senile plaques parallel duration and severity of Alzheimer's disease. Neurology 42:631–639.

Barria A, Muller D, Derkach V, Griffith L, Soderling T (1997) Regulatory phosphorylation of AMPA-type glutamate receptors by CaM-KII during long-term potentiation. Science 276:2042–2045.

Behrends J, Ten Bruggencate G (1993) Cholinergic modulation of synaptic inhibition in the guinea pig hippocampus in vitro: excitation of GABAergic interneurons and inhibition of GABA-release. J Neurophysiol 69:626–629.

Bell K, Shim H, Chen C-K, McQuiston A (2011) Nicotinic excitatory postsynaptic potentials in hippocampal CA1 interneurons are predominantly mediated by nicotinic receptors that contain $\alpha 4$ and $\beta 2$ subunits. Neuropharmacology 61:1379–1388.

Bell L, Bell K, McQuiston A (2015) Activation of muscarinic receptors by ACh release in hippocampal CA1 depolarizes VIP but has varying effects on parvalbumin-expressing basket cells. J Physiol 593:197–215.

Burnashev N, Zhou Z, Neher E, Sakmann B (1995) Fractional calcium currents through recombinant GluR channels of the NMDA, AMPA and kainate receptor subtypes. J Physiol 485:403–418.

Castro N, Albuquerque E (1995) alpha-Bungarotoxin-sensitive hippocampal nicotinic receptor channel has a high calcium permeability. Biophys J 68:516–524.

Chatzikalymniou A, Skinner FK (2018) Deciphering the contribution of oriens-lacunosum/moleculare (OLM) cells to intrinsic theta rhythms using biophysical local field potential (LFP) models. eNeuro 5:ENEURO.0146-18.2018.

Chevalerye V, Piskorowski R (2014) Modulating excitation through plasticity at inhibitory synapses. Front Cell Neurosci 8:93.

Collingridge G, Kehl S, McLennan H (1983) Excitatory amino acids in synaptic transmission in the Schaffer collateral-commissural pathway of the rat hippocampus. J Physiol 334:33–46.

Dajas-Bailador F, Mogg A, Wonnacott S (2002) Intracellular Ca2+ signals evoked by stimulation of nicotinic acetylcholine receptors in SH-SY5Y cells: contribution of voltage-operated Ca2+ channels and Ca2+ stores. J Neurochem 81:606–614.

Desikan S, Koser D, Neitz A, Monyer H (2018). Target selectivity of septal cholinergic neurons in the medial and lateral entorhinal cortex. Proc Natl Acad Sci U|S|A 115:E2644–E2652.

Destexhe A, Mainen Z, Sejnowski T (1998) Kinetic models of synaptic transmission. In: Methods in neuronal modeling: from ions to networks (Koch C, Segev I, eds). Cambridge, MA: MIT.

Fabian-Fine R, Skehel P, Errington ML, Davies HA, Sher E, Stewart MG, Fine A (2001) Ultrastructural distribution of the $\alpha 7$ nicotinic acetylcholine receptor subunit in rat hippocampus. J Neurosci 21:7993–8003.

Gradinaru V, Zhang F, Ramakrishnan C, Mattis J, Prakash R, Diester I, Goshen I, Thompson KR, Deisseroth K (2010) Molecular and cellular approaches for diversifying and extending optogenetics. Cell 141:154–165.

Graupner M, Brunel N (2005) STDP in a bistable synapse model based on CaMKII and associated signaling pathways. PLoS Comput Biol 3:e221.

Graupner M, Brunel N (2012) Calcium-based plasticity model explains sensitivity of synaptic changes to spike pattern, rate, and dendritic location. Proc Natl Acad Sci U S A 109:3991–3996.

Graupner M, Maex R, Gutkin B (2013) Endogenous cholinergic inputs and local circuit mechanisms govern the phasic mesolimbic dopamine response to nicotine. PLoS Comput Biol 9:e1003183.

Griguoli M, Cherubini E (2012) Regulation of hippocampal inhibitory circuits by nicotinic acetylcholine receptors: nAChRs and inhibitory circuits in the hippocampus. J Physiol 590:655–666.

Gu Z, Yakel J (2011) Timing-dependent septal cholinergic induction of dynamic hippocampal synaptic plasticity. Neuron 71:155–165.

Gu Z, Yakel J (2017) Inducing theta oscillations in the entorhinal hippocampal network in vitro. Brain Struct Funct 222:943–955.

Gu Z, Alexander G, Dudek S, Yakel J (2017) Hippocampus and entorhinal cortex recruit cholinergic and NMDA receptors separately to generate hippocampal theta oscillations. Cell Rep 21:3585–3595.

Gu Z, Smith KG, Alexander GM, Guerreiro I, Dudek SM, Gutkin B, Jensen P, Yakel JL (2020) Hippocampal interneuronal $\alpha 7$ nAChRs modulate theta oscillations in freely moving mice. Cell Rep 31:107740.

Haam J, Yakel J (2017) Cholinergic modulation of the hippocampal region and memory function. J Neurochem 142:111–121.

Hasselmo ME (2006) The role of acetylcholine in learning and memory. Curr Opin Neurobiol 16:710–715.

Hasselmo ME, Schnell E, Barkai E (1995) Dynamics of learning and recall at excitatory recurrent synapses and cholinergic modulation in rat hippocampal region CA3. J Neurosci 15:5249–5262.

Higgins D, Graupner M, Brunel N, Latham P (2014) Memory maintenance in synapses with calcium-based plasticity in the presence of background activity. PLoS Comput Biol 10:e1003834.

Hodgkin A, Huxley A (1952) A quantitative description of membrane current and its application to conduction and excitation in nerve. J Physiol 117:500–544.

Lüscher C, Malenka R (2012) NMDA receptor-dependent long-term potentiation and long-term depression (LTP/LTD). Cold Spring Harb Perspect Biol 78:a005710.

Leão RN, Mikulovic S, Leão KE, Munguba H, Gezelius H, Enjin A, Patra K, Eriksson A, Loew LM, Tort ABL, Kullander K (2012) OLM interneurons differentially modulate CA3 and entorhinal inputs to hippocampal CA1 neurons. Nat Neurosci 15:1524–1530.

Levin E (2002) Nicotinic receptor subtypes and cognitive function. J Neurobiol 53:633–640.

Müller C, Remy S (2014) Dendritic inhibition mediated by O-LM and bistratified interneurons in the hippocampus. Front Synaptic Neurosci 6:23.

Maccaferri G, David J, Roberts B, Sxucs P, Cottingham CA, Somogyi P (2000) Cell surface domain specific postsynaptic currents evoked by identified GABAergic neurones in rat hippocampus in vitro. J Physiol 524:91–116.

McKay B, Placzek A, Dani J (2007) Regulation of synaptic transmission and plasticity by neuronal nicotinic acetylcholine receptors. Biochem Pharmacol 74:1120–1133.

McQuiston A, Madison D (1999) Nicotinic receptor activation excites distinct subtypes of interneurons in the rat hippocampus. J Neurosci 19:2887–2896.

Meredith R, Floyer-Lea A, Paulsen O (2003) Maturation of long-term potentiation induction rules in rodent hippocampus: role of GABAergic inhibition. J Neurosci 23:11142–11146.

Mikulovic S, Restrepo CE, Siwani S, Bauer P, Pupe S, Tort ABL, Kullander K, Leão RN (2018) Ventral hippocampal OLM cells control type 2 theta oscillations and response to predator odor. Nat Commun 9:3638.

Nicholson E, Kullmann D (2021) Nicotinic receptor activation induces NMDA receptor independent long-term potentiation of glutamatergic signalling in hippocampal oriens interneurons. J Physiol 599:667–676.

Ormond J, Woodin MA (2009) Disinhibition mediates a form of hippocampal long-term potentiation in area CA1. PLoS One 4:e7224.

Parikh V, Kozak R, Martinez V, Sarter M (2007) Prefrontal acetylcholine release controls cue detection on multiple time scales. Neuron 56:141–154.

Patil MM, Hasselmo ME (1999) Modulation of inhibitory synaptic potentials in the piriform cortex. J Neurophysiol 81:2103–2118.

Patil MM, Linster C, Lubenov E, Hasselmo ME (1998) Cholinergic agonist carbachol enables associative long-term potentiation in piriform cortex slices. J Neurophysiol 80:2467–2474.

Pitler T, Alger B (1992) Cholinergic excitation of GABAergic interneurons in the rat hippocampal slice. J Physiol 450:127–142.

Rinzel J (1985). Bursting oscillations in an excitable membrane model. In: Ordinary and partial differential equations: proceedings of the 8th conference held at Dundee, Scotland, 1984 (Sleeman BD, Jarvis RJ, eds), pp 304–316. New York: Springer.

Rotstein HG, Pervouchine DD, Acker CD, Gillies MJ, White JA, Buhl EH, Whittington MA, Kopell N (2005) Slow and fast inhibition and h-current interact to create a theta rhythm in a model of CA1 interneuron network. J Neurophysiol 94:1509–1518.

Rubin JE, Gerkin RC, Guo-Qiang Bi, Chow CC (2005) Calcium time course as a signal for spike-timing-dependent plasticity. J Neurophysiol 93:2600–2613.

Sabatini BL, Oertner TG, Svoboda K (2002) The life cycle of Ca(2+) ions in dendritic spines. Neuron 33:439–452.

Saudargienė A, Graham BP (2015) Inhibitory control of site-specific synaptic plasticity in a model CA1 pyramidal neuron. Biosystems 130:37–50.

Schmid LC, Mittag M, Poll S, Steffen J, Wagner J, Geis H-R, Schwarz I, Schmidt B, Schwarz MK, Remy S, Fuhrmann M (2016) Dysfunction of somatostatin-positive interneurons associated with memory deficits in an Alzheimer's disease model. Neuron 92:114–125.

Schneggenburger R, Forsythe ID (2006) The calyx of Held. Cell Tissue Res 326:311–337.

Schulz JM, Knoflach F, Hernandez M-C, Bischofberger J (2018) Dendrite-targeting interneurons control synaptic NMDA-receptor activation via nonlinear α5-GABA$_A$ receptors. Nat Commun 9:3576.

Shouval H, Bear M, Cooper L (2002) A unified model of NMDA receptor-dependent bidirectional synaptic plasticity. Proc Natl Acad Sci U S A 99:10831–10836.

Tsuneki H, Klink R, Lena C, Korn H, Changeux J (2000) Calcium mobilization elicited by two types of nicotinic acetylcholine receptors in mouse substantia nigra pars compacta. Eur J Neurosci 12:2475–2485.

Vernino S, Rogers M, Radcliffe K, Dani J (1994) Quantitative measurement of calcium flux through muscle and neuronal nicotinic acetylcholine receptors. J Neurosci 14:5514–5524.

Wigström H, Gustafsson B (1985) Facilitation of hippocampal long-lasting potentiation by GABA antagonists. Acta Physiol Scand 125:159–172.

Witten IB, Lin S-C, Brodsky M, Prakash R, Diester I, Anikeeva P, Gradinaru V, Ramakrishnan C, Deisseroth K (2010) Cholinergic interneurons control local circuit activity and cocaine conditioning. Science 330:1677–1681.

Yakel J (2012) Nicotinic ACh Receptors in the hippocampus: role in excitability and plasticity. Nicotine Tob Res 14:1249–1257.

Yang GR, Murray JD, Wang X (2016) A dendritic disinhibitory circuit mechanism for pathway-specific gating. Nat Commun 7:12815.

Young GW, Keizer J (1992) A single-pool inositol 1,4,5-trisphosphate-receptor-based model for agonist-stimulated oscillations in Ca2+ concentration. Proc Natl Acad Sci U S A 89:9895–9899.